Development of Advanced Multifunctional Polymer Binders for Cathode Materials in Lithium-Ion Batteries

Adam Schmidt

Honors Research Thesis

3/29/18

Department of Mechanical and Aerospace Engineering

Advisor: Dr. Jung Hyun Kim

Abstract

Reducing costs and improving environmental friendliness for the manufacturing processes of lithium-ion (Li-ion) battery cells are important goals of today's battery research. Presently, the industry standard polyvinylidene fluoride (PVdF) binder – the glue holding the electrode together – requires a toxic solvent, N-methylpyrrolidone (NMP), during the electrode fabrication processes. Since the purchase and proper disposal of NMP contributes about 13% of the total cost for Li-ion battery production, finding a water-soluble replacement for PVdF would be economically beneficial. The purpose of this research is to develop an effective binder material that uses a water-based solvent, so that currently used toxic solvents can be eliminated, reducing cost and increasing environmental friendliness. Lithiated polyacrylic acid (LiPAA), an alternative binder, uses a water-based solvent and has other desirable properties, such as increased adhesion force, increased cycle life, and decreased capacity fade. LiPAA is not currently a feasible binder, however, because cathodes produced using LiPAA are particularly brittle, which causes cracking during the manufacturing process, leading to reduced cycle life. In order to alleviate this undesirable mechanical behavior, LiPAA will be doped with styrene-butadiene rubber (SBR) and sodium alginate (Na-Alg). We hypothesize that adding these materials to LiPAA will provide the electrode with the desirable electrochemical properties of LiPAA, while mitigating cracking. We applied various compositions of LiPAA, Na-Alg, and SBR binders to a $LiNi_{0.5}Mn_{1.5}O_4$ cathode. We assessed the quality of the coating and microstructure using scanning electron microscopy (SEM). We fabricated cathodes with different binders into coin-type Li-ion battery cells to measure electrochemical performance. We examined the effects of binder composition on the physical and electrochemical properties of cathodes in Li-ion batteries. We found that Na-Alg reduces brittle

fracture in the cathodes using LiPAA, where SBR exacerbates it. Increasing the Na-Alg content was found to drastically increase the capacity fade experienced in a full cell.

Acknowledgements

This research is the culmination of the hard work of many people, not just myself. First and foremost, I would like to thank Dr. Jung Hyun Kim. Dr. Kim took me on as an undergraduate researcher only a few weeks into his time here at Ohio State back in September 2016. We have learned how to navigate the undergraduate research process here at OSU together, and his guidance on the direction of this project as well as his generosity and willingness to teach the content to me has been invaluable throughout our time together.

Cody O'Meara, a graduate student under Dr. Kim also deserves special recognition. Cody trained me on most equipment including the Arbin Cycler, and Glove Box. He helped with data collection including SEM image gathering, and providing the software for electrochemical data plotting. Cody was available at all hours to help troubleshoot equipment problems, optimize the cathode creation process, and analyze data. This research truly would not have been possible without him.

Thanks also to the rest of graduate and undergraduate students in Dr. Kim's lab who each provided nudges in the right direction, by running small tests or knowing where certain equipment was located. My friends and family should be thanked as well. They've allowed me to practice presentations, and continually lend an ear to my research efforts over the past year and a half.

Table of Contents

List of Figures

List of Tables

Chapter 1: Introduction

1.1 Historical Background of Lithium Ion Batteries and Cathode Components

Lithium Ion (Li-Ion) batteries, first introduced commercially in 1991 by Sony Corporation, revolutionized the portable electronics market. These batteries were safer and had higher specific energies than Li-Metal batteries, as well as lower environmental impacts than the current state of the art Nickle Cadmium batteries [1]. Li-Ions were quickly iterated upon to improve energy density by testing new cathode and anode materials as well as process functions such as slurry quality, casing performance, and adhesion to current collectors [1]. Cathodes materials in particular garnered a lot of attention since these materials have a large impact on the overall power, capacity, and safety of the battery. Eventually $LiCoO_2$ emerged as the most commercialized cathode material, in part because of its relatively high theoretical specific capacity of 274 mAh/g and acceptable voltage vs. Lithium of 3.8 V [2]. It continues to be a common cathode material today. Due to the size of active material particles, a conductive additive was necessary in order to decrease internal resistances in the cathode by facilitating the flow of electrons. Carbon black nanoparticles commonly fill this role today [3]. In order to ensure that the two components exhibited appropriate adhesion to one another and the current collector, a binder, most notably PVdF [4], became standard in every cathode. While the materials characterizing the most successful Li-Ion batteries have changed drastically in the past 27 years, the components of the cathode – Active materials, carbon conductors, and binders – have not.

In a Li-Ion battery cell, a cathode, which by definition contains Li ions, is paired with an anode. While the battery is charging, a current is provided in order to transfer Li ions from the

cathode, through the electrolyte to be stored within the anode, a process known as intercalation [5]. When the cell is discharged, or used, the Li ions transfer back to the cathode through the electrolyte, called deintercalation. It is this reversible process that makes Li-Ion batteries rechargeable, which is why they are so prevalent in today's portable electronics such as phones, power tools, and electric vehicles (EVs) [6]. Additional components such as the separator, current collectors, and casing, shown in Figure 1, play a critical role in the making the battery operational, but only a small role in its performance.

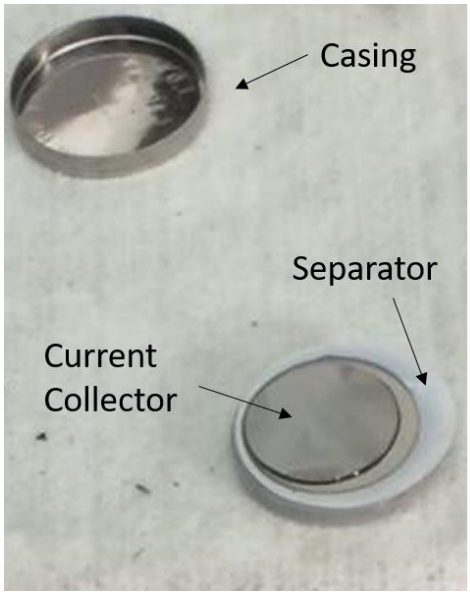

Figure 1: Inactive Components of a Coin Cell

For this reason, the majority of Li-Ion battery research has focused on developing the cathode and anode to increase the battery's specific capacity (both gravimetric and volumetric), cycle life, potential difference, and safety, while reducing cost, capacity fade, and impedance, among other things [5].

As mentioned above, cathodes (and anodes) consist of three parts: active material, carbon conductors, and binder material. A representation is shown in Figure 2.

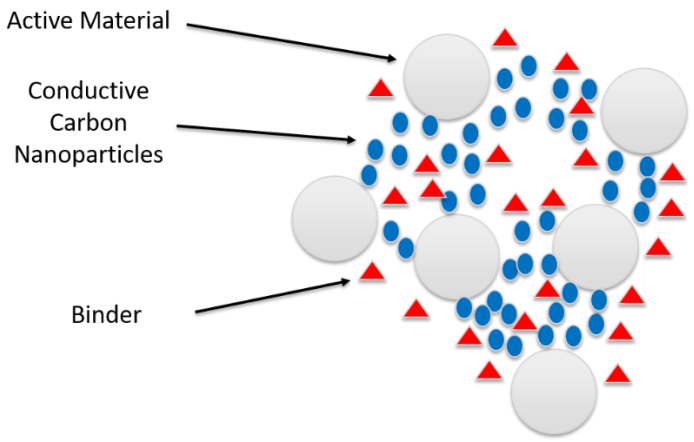

Figure 2: Representation of Cathode Composition (not to scale)

Both the composition of and ratio between these components are the subject of research throughout the industry. New materials with exciting potential are often being discovered, however, they can rarely be implemented without intense research to solve their current complications. Silicon as an anode material is a perfect example of this. Despite having the potential to increase the capacity of Li-Ion batteries by a factor of 10, expansion of the Si particles during intercalation creates a problem that has yet to be overcome in a way that is compatible with commercialization [7]. Problems with the binder that this study focused on, Lithiated Poly Acrylic Acid (LiPAA) also prevent commercialization.

LiPAA is a binder material that was first developed in 2007 by 3M Innovative Properties company [8], for use in anodes. In 2015, Kim and others showed that it could be used to create a Cathode Electrolyte Interface, or CEI on high voltage cathodes such as $LiNi_{0.5}Mn_{1.5}O_4$ (LNMO) [9], which would prevent a decomposition reaction with the electrolyte from occurring. This CEI formation opens up new avenues of research, by allowing many additional cathode materials – which were previously impossible to use due to this decomposition reaction – to be considered. LNMO has a voltage of 4.7 V vs. Lithium [10], about 0.9 V higher than the 3.8 V for $LiCoO_2$

cathodes, the industry standard [2]. This increased voltage allows the battery to provide additional power to the load.

In addition to creating an effective CEI, LiPAA provides other useful functionalities. The current industry standard cathode binder, polyvinylidene fluoride (PVdF), requires a toxic solvent, N-methylpyrrolidone (NMP), for activation [11]. Though this solvent is removed during the manufacturing process, reclamation can be expensive. In fact, in industry standard Li-Ion batteries, the proper purchase, transportation, reclamation, and disposal of NMP account for about 14% of the total cost of the battery [12], even though it isn't even contained in the final product. LiPAA has the benefit of using water as its solvent [9], instead of NMP. Not only does this make LiPAA environmentally friendly, but it also reduces the cost of the battery by about 13% [12], because water can be evaporated off without an expensive reclamation process, and is much cheaper than NMP to purchase. Further, the Li ions within LiPAA, in addition to the Li ions composing LNMO, are intercalated during charging, which provides 30% more lithium ions compared to an industry standard cathode [9]. This reduces the capacity fade of the battery leading to longer cell life. LiPAA also has a higher adhesion force – a measurement of how strong the binding properties are – than PVdF [9], ensuring that it adequately replicated the current binder's functionality.

Despite these exceptional benefits, LiPAA has yet to be implemented commercially, because it causes the surface of the cathode to crack during manufacturing The mechanical degradation of the cathode leads to an extreme drop in cycle life and inevitably, total cell failure [13]. It was hypothesized that materials with effective binder properties that were also water soluble could be combined with LiPAA in various weight ratios in order to alleviate the brittle cracking exhibited by LiPAA, while retaining its benefits such as CEI formation, increased cycle

life, water solubility, and decreased cost. Through extensive literature review sodium alginate (Na-Alg) and styrene-butadiene rubber (SBR) were determined to have met these criteria, and thus were chosen to be combined with LiPAA in this experiment [14–16].

1.2 Focus of Thesis

The purpose of this project was to test the mechanical and electrochemical properties of cathodes utilizing systematically chosen binder combinations of LiPAA with Na-Alg, and LiPAA with SBR. The tests, which will be described in the Methodology, were used to determine which combination, if any, of binder materials provides adequate crack reduction in the cathode, while retaining the benefits of using LiPAA as a binder.

1.3 Significance of Research

In a market of constantly expanding portable electronics, reducing the cost of Li-Ion batteries is an important consideration in making sure that a product is successful. As these portable electronics increase in functionality they will inevitable require more power, and thus it is crucial for power density to be improved as well. The automotive industry exemplifies a marriage of these two constraints.

Transitioning to EVs which are powered by Li-Ion batteries, is an important environmental step for auto manufacturers. In order to make EVs competitive in the automotive market, it is imperative that manufacturers seek to reduce the cost of EVs by reducing the cost of the Li-Ion batteries that they use. Li-ion batteries contribute approximately 25% to the total cost of an EV [17]. At the same time, the performance of the EV, including overall lifetime and distance to travel on a full charge, cannot be sacrificed. This makes improving the specific capacity and decreasing the capacity fade of Li-Ion batteries as necessary as reducing their cost.

In addition to the automotive industry, Li-Ion batteries are a limiting factor in achieving widespread onsite power generation from renewable energies such as solar, or wind. Because the amount of energy being collected from solar and wind is dependent on the amount of sunlight, or wind available at that particular time, the energy needs to be stored somehow so that it can be used when it isn't being generated. Li-Ion batteries represent the best storage potential for this excess energy [18]. Energy storage is also an important consideration in making sure that peak energy demand can be met. Without Li-Ion batteries to store the energy, it is impossible for the grid to use an amount of energy greater than is being produced at any given time.

By conducting this study to determine an effective way to utilize LiPAA in cathodes, we help to reduce the cost of Li-Ion batteries and increase their energy density, which is directly in line with facilitating the development of EVs and clean energy technologies. Additionally, the water-soluble nature of LiPAA has a positive environmental impact, which works towards the same goal as the electric vehicle and clean energy industries.

1.4 Overview of Thesis

This thesis consists of 5 chapters. Chapter 2 will discuss the material, and cathode composition selection process. Chapter 3 will discuss the methodology and experimental setup of this research. Chapter 4 will focus on the results of the research including multiple SEM images examining the extent of cracking exhibited, as well as including a cycle life analysis for each of the compositions. Chapter 5 will provide a conclusion for this thesis, and recommend new avenues for research in the future.

Chapter 2: Material Selection

2.1 Materials

As mentioned in the previous section, cathodes using LiPAA as a binder become brittle during manufacturing when they are dried. The first step in creating a cathode that overcomes this issue was to choose and assemble the correct components. The components of the cathode are as follows: active material, conductive carbon nanoparticles, binder particles, solvent, and the current collector. In addition, the equipment necessary to synthesize these components together: Dr. Blade, and a vacuum oven, shown in Figures 3 and 4 respectively, had to be purchased or located.

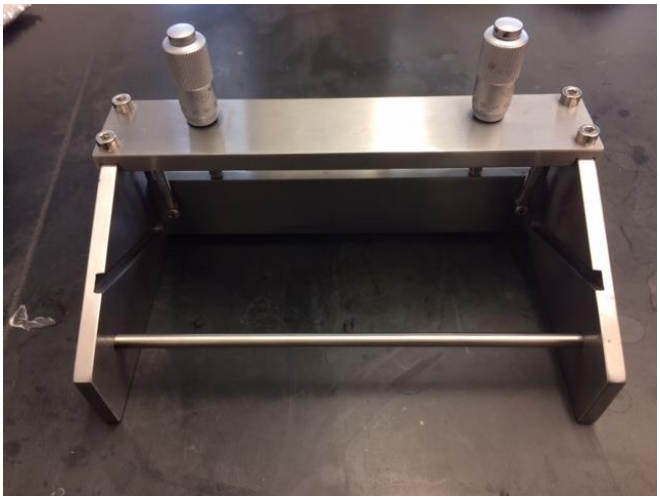

Figure 3: Dr. Blade - height adjustable thin film spreader

Figure 4: Vacuum Oven

Obtaining this equipment and the conductive carbon nanoparticles was relatively straightforward. Since it is known that LiPAA is soluble in water, no preparation was required to obtain the solvent. For the binder and active material however, important decisions were made as to their composition and quantity.

2.1.1 Binder Material Selection

The most important decision was determining which alternative binder materials could be paired with LiPAA that would potentially reduce cracking issues. It was hypothesized that binders exhibiting high elasticity could appropriately improve the brittle qualities of LiPAA. An additional, and rigid, constraint was that this binder must be water soluble. While it is possible to pair more than one binder material together, having more than one solvent causes unwanted side reactions leading to battery failure.

Na-Alg has been used as a binder in both cathodes and anodes in recent years. It is often used alone, and has furthered the development of non-fluorinated cathodes [19] and silicon/graphite anodes [20]. Due to its water soluble nature and superior electrochemical performance [19] it was hypothesized that combining it with LiPAA could help reduce cracking while maintaining

excellent electrochemical results. Therefore, Na-Alg was chosen to be paired with LiPAA as a binder in this experiment.

SBR is currently used as a binder in both cathodes and anodes in Li-ion battery research. It is often used in combination with carboxyl-methyl-cellulose (CMC). In these combinations SBR is the primary binder, and CMC acts as a thickening agent [21]. Since SBR has achieved widespread effectiveness as a water soluble anode binder, it was hypothesized that combining it LiPAA would bind the cathode together more strongly, thus reducing brittle fracture [15,16,21]. Therefore, SBR was chosen to be paired with LiPAA as a binder in this experiment.

2.1.2 Active Material Selection

The active material used for this cathode was also carefully chosen. Though LiPAA is useful as a binder in low voltage cathodes (< 4.5 V) [13], it is most suited for use with high voltage cathodes (>4.5V), because the CEI that it creates works as a passivating layer against unwanted electrolysis reactions between the cathode and electrolyte [9]. Because of this, it was determined that LiPAA should be tested using a high voltage cathode. LNMO (4.7 V vs Li) was chosen because it had been used in Dr. Kim's previous study of LiPAA, so it's documented properties were measured in an LNMO cathode. Because using LiPAA as a cathode binder is a recent innovation – the first paper to attempt this was published in 2015 – there are few other documented examples of high voltage cathodes using LiPAA as a binder. For the sake of consistency of data in literature, and continuity with Dr. Kim's research LNMO was chosen as the active material in this.

For cost reasons, the LiPAA used in this experiment was synthesized rather than purchased. Poly acrylic acid (PAA) and lithium hydroxide (LiOH), were combined to a pH of ~7

in aqueous solution to ensure that the appropriate neutralization reaction had occurred [9]. A 10 wt% solution of LiPAA was synthesized for use in cathode creation.

2.2 Binder Ratio Selection

The next step was to choose the ratio of LiPAA to either Na-Alg or SBR by weight percent. In order to obtain appropriate data it was determined that the ratios would be 100:0, 70:30, 60:40, 50:50, 40:60, 30:70, and 0:100. Solutions of each binder combination at these weight percents were then created by adding the appropriate amount of Na-Alg or SBR and water to the 10 wt% LiPAA solution. The solutions were left on a magnetic stir plate overnight to ensure thorough mixing. These new solutions were extremely viscous, and thus were created at 3.75 wt%. This ensured that the binder and solvent could be easily added to the active material and carbon conductors during cathode synthesis without adding excess solvent.

2.3 Cathode Composition Ratio Selection

Choosing the ratio of active material, to conductive carbon particles, to binder is also an important component in the development of a cathode. It is generally accepted in literature that the active material should compose as much of the overall cathode as possible without sacrificing the electrochemical or mechanical advantages provided by the carbon conductors, and binder. With large scale manufacturing this composition often contains over 90% active material by weight. This ratio uses as little conductive material and binder as possible leaving minimum room for error. Since cathode creation in this experiment took place on a lab scale, it was wise to provide slightly more room for error. It was then determined that an 85% active material, 7.5% conductive carbon nanoparticle, and 7.5% binder material (by weight), would appropriately

minimize the porosity of the cathode to provide relevant results while allowing enough error for a lab setting.

Chapter 3: Methodology

3.1 Cathode Creation

For Li-Ion batteries in a large-scale manufacturing setting, components are measured autonomously and cathodes with perfected formulas are created in huge batches. On a lab-scale where each iteration of the cathode is slightly different, all chemicals were measured by hand, and created individually rather than in batches. This allowed the composition of the cathodes to be as close to the desired ratios as possible, while not wasting expensive resources. After measuring out the active material, conductive carbon particles, and the binder into a mortar, the solvent, in this case water, was added. A pestle was used to grind and homogenize the mixture known as a slurry after the addition of the solvent. After 5 minutes of grinding, the slurry was placed into a vacuum chamber for 2 ½ minutes in order to remove any air pockets that might have formed during the previous step. The slurry was then scooped onto the already prepared current collector. In this case, since a cathode was created, the current collector was a thin piece of aluminum foil [22]. The current collector was prepared by tightly adhering it to a sheet of glass using ethanol. The slurry was then spread uniformly across the surface of the current collector with the use of Dr. Blade. Dr. Blade, holds a blade a set distance from the surface it is sitting on. Micrometers attached to the instrument allow the height to be read or adjusted. After spreading, the cathode was placed in a vacuum at 90° C for approximately 30 minutes, or until the cathode is completely dry. The vacuum oven removes the solvent from the cathode so that it

doesn't react with the other components once the battery was fabricated. After the cathode dried, 13.7 mm diameter samples are punched out and weighed to determine their active mass.

In preparation for the final samples, many cathodes were created in order to optimize the lab-scale development process. Solvent to dry mass ratio, grinding time, pre-spreading vacuum chamber time, and the height of Dr. Blade were all independently tested. Visual inspection was used to determine which combination of these variables produced the highest quality surface coating. In addition to surface coating quality, reducing the thickness of the vacuum dried cathode was an important factor, because increased thickness can lead to increased impedance and decreased mechanical properties [23]. Since moisture evaporates from the cathode during vacuum drying, the thickness of a dry cathode is less than the height at which Dr. Blade was set. One way to account for this thickness difference is to measure the active mass in each 13.7 mm diameter sample. In order to reduce the thickness appropriately, but keep it large enough that it could be paired with a good quality anode for a full cell, the target active mass of each sample was between 8 and 15 mg. The combination of the aforementioned variables that produced both high quality surface coatings, and samples with an active mass between 10 and 15 mg are as follows: 2:1 solvent to dry mass ratio, 5 minutes of grinding time in the mortar, 2 ½ minutes of time in a vacuum chamber before spreading, and a height of 300 μm for Dr. Blade.

All the variables that were optimized are standard lab practice except for placing the slurry in a vacuum chamber before spreading it. The expressed purpose of this vacuum chamber time was to remove air bubbles from the slurry which were hypothesized to be causing defects in the coating quality as shown in Figure 5.

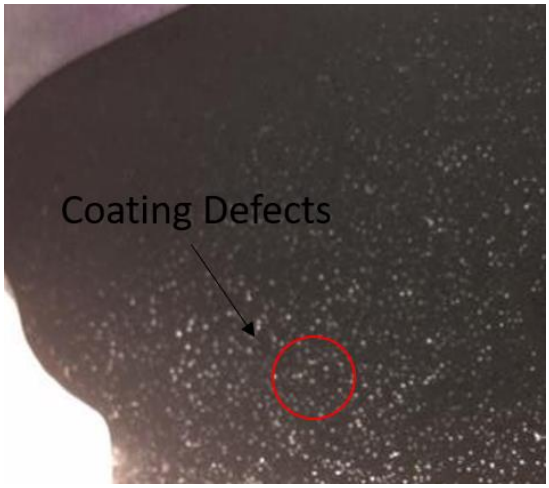

Figure 5: A pre-optimized cathode (LiPAA) with coating defects possibly due to air bubbles

Though it appeared that the vacuum chamber did not entirely eliminate the defects as shown in Figure 6 it did significantly reduce them. This is evidence to support the hypothesis that tiny air bubble can cause surface defects while drying, and that a short vacuum can reduce this problem. This is significant and should be widely noted by researchers moving forward.

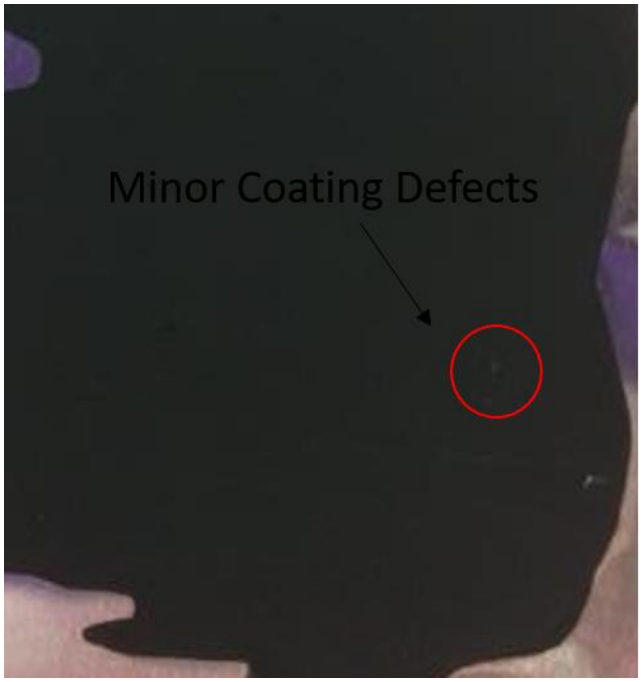

Figure 6: Minor defects in a final cathode (LiPAA)

Anyone familiar with Li-Ion batteries knows that it is important to only create cathodes on days with low relative humidity. This is because PVdF is so reactive with water, that exposing it to the air on a rainy day during cathode synthesis will result in premature failure of the battery. It should be noted that LiPAA uses water as its solvent, and thus its performance is not negatively affected by exposure to humid air. Therefore, there was no need to take weather into consideration when the cathodes samples were created.

3.2 Anode Library Creation

Batteries have both a cathode and an anode, so after creating all cathode samples with an acceptable quality, anodes samples to pair with them were created. Anodes have the same components as cathodes – active material, carbon conductors, a binder, and solvent – but require a different active material. In order to isolate the changes made in the cathode, the industry standard anode was created for use in this experiment. It is composed of Graphite, conductive carbon nanoparticles, and PVdF binder in an 89%, 3%, 8% ratio respectively.

Cathode and anode samples each have a capacity that can be calculated based on the chemistry of the active mass, and mass of the sample using Equation 1.

$$Capacity = Specific\ Capacity * Active\ Mass \tag{1}$$

Where specific capacity is calculated from molar mass using Equation 2.

$$Specific\ Capacity = \frac{96{,}485\ C}{mol} * \frac{1\ A{*}s}{C} * \frac{1\ hr}{3600\ s} * \frac{1000\ mA}{A} * \frac{1\ mol\ (Active\ Mass}{g} \tag{2}$$

For example, an LNMO cathode sample with a mass of 10 mg:

$$Specific\ Capacity\ LNMO = \frac{96{,}485\ C}{mol} * \frac{1\ A{*}s}{C} * \frac{1\ hr}{3600\ s} * \frac{1000\ mA}{A} * \frac{1\ mol\ LNMO}{182.7g} = 146.7\frac{mAh}{g}$$

$$Capacity\ LNMO\ Sample = 146.7 \frac{mAh}{g} * .010\ g = 1.46\ mAh$$

In order for the battery to function as normal, the anode sample must have the same capacity as the cathode sample. Knowing this, it is possible to calculate the required active mass of the anode sample to match the cathode. Since the active mass of each sample can vary, even when spread at the same thickness, an anode library was created. The purpose of this library was to have many anode samples with an appropriate range of active masses, such that regardless of the exact cathode sample, a matching anode sample would be readily available. Knowing that acceptable cathode samples would fall in the range of 10-15 mg of active mass, it was calculated that the mass of each anode sample would be 4.5 - 6.8 mg using Equation 1.

The Anode library was created using a very similar process to the cathode creation explained in Section 2.2, with a few minor changes. Since it is not standard practice to vacuum dry the anode slurry before spreading it, this step used during cathode creation was ignored. As mentioned above, the anode uses PVdF as a binder, and consequentially NMP as the solvent. This means that humid weather would in fact introduce defects into the anode. Accordingly, the anodes were created on a dry cloudless day with relatively low humidity. The slurry was created using an 89%, 3%, 8% active mass, carbon conductors, binder ratio. A 2:1 solvent to dry mass ratio was used. Anodes are coated onto copper, rather than aluminum, foil as the current collector. Anodes were created with the height of Dr. Blade as 100, 130, 150, 180, 200, and 230 μm.

3.3 Coin Cell Creation

After creating the cathode and anode samples, coin cells were fabricated in order to perform electrochemical testing. Coin cells, small circular batteries primarily used to collect

electrochemical data, consist of the cathode and anode, each coated onto the current collector, with an $LiPF_6$ electrolyte and a separator between them. Spacers and a small spring help to ensure the electrodes fully contact each other. All components are housed in a casing that is crimped shut. Since many of the components may be reactive with air, all coin cells are fabricated inside an argon filled glove box, shown below in Figure 7. A cell with these components is known as a full cell.

Figure 7: Argon Filled Glove Box

Another type of coin cell, more often used for proof of concept research purposes is known as a half cell. Half cells differ from full cells in that they use lithium metal as the anode rather than the mixture described in section 2.3. This provides an easy way to test cathode functionality, but is not representative of commercialized Li-ion batteries. Using lithium metal as the anode facilitates the growth of dendrites, which can dangerously short circuit a cell when using commercially viable amperage [24]. Though it is not dangerous to test on a research scale, the lithium metal provides an additional source of lithium to the cathode and thus masks

scavenging reactions that deplete the cathodes lithium supply and cause capacity fade in the battery. For this reason, it was decided that both a half and a full cell for each cathode chemistry would be created and tested.

Once coin cells have been fabricated, they are tested using an Arbin Cycler shown below in Figure 8.

Figure 8: Arbin Cycler

Using the Arbin software, these coin cells are charged and discharged at a specific 'C rate,' which is determined using Equation 3 below.

$$1C\ (A) = Active\ mass\ (g) * specific\ capacity\ \left(\frac{mAh}{g}\right) * \frac{1A}{1000mA} \quad (3)$$

Where 1C denotes the total amperage to be charged and discharged during each cycle. A C rate of C/1, means that the calculated amperage to full charge will be delivered to the battery over 1 hour. The C rate for all cells cycled during this experiment was: C/20 for cycle 1, C/10 for cycle 2, and C/5 charging and C/2 discharging from cycle 3 onward. Slowly cycling the battery during the first cycles allows lithium to be fully intercalated in the anode, and a high quality Solid

Electrolyte Interface (SEI) to form. The cells were then left to cycle for about two weeks to collect data.

3.4 SEM Imaging

While the Arbin Cycler provides electrochemical data for each cathode sample it does not test mechanical properties. In order to get a closer look at the level cracking that occurred, Scanning Electron Microscopy (SEM) was used. Before SEM imaging can occur, samples to be imaged must be coated using a Hummer VI Sputter shown below in Figure 9. The samples are then placed in a chamber and bombarded with electrons. The resulting image is constructed from the electron scattering patterns.

Figure 9: Hummer VI Sputter

Since SEM imaging requires that the surface be coated, coin cells could not be created using these exact samples. The samples imaged however, were created in the same small batch as the samples from which half and full cells were fabricated. This means that the cracking exhibited by the imaged samples is representative of the cracking that occurred in cathodes from which electrochemical data was taken.

SEM images were taken of each sample at 100x and 250x magnitudes. An analysis software called ImageJ was used to determine what percentage of the area of the cathode was cracked. It functions by turning a greyscale SEM image to black and white. The user chooses the threshold for this cutoff. Since cracks are in shadow in SEM images, they show up as darker than the particles composing the cathodes. Using an image where all cracks are black, and everything else is white, ImageJ then calculates the percentage of the total area that is blacked out, providing qualitative data for crack density. The results of this analysis and the others mentioned above will be provided in the following chapter.

Chapter 4: Results

4.1 Mechanical Results

The surface coating quality was analyzed, first by inspection, and then using SEM. A reduction in brittle fracture was the desired result of the mechanical analysis.

4.1.1 Surface Quality by Inspection

As cathodes were created, the quality of the surface coating was inspected visually. Cathodes with apparent cracks, or pores were each remade to ensure the best quality possible in the final samples. During this process it was apparent that cathodes using only LiPAA as a binder suffered severely from cracking, such that the current collector could be seen through the cathode as shown in Figure 10. The pure Na-Alg cathode on the other hand exhibited very little cracking as seen in Figure 11.

Figure 10: Pure LiPAA Cathode with cracking

Figure 11: Pure Na-Alg Cathode with few pores

However, when attempting to create cathodes using SBR it was immediately obvious that SBR was degrading the quality of surface coating not enhancing it as expected. Figure 12 shows this severe degradation. Creating a cathode using only SBR as the binder produced similarly disastrous results as shown in Figure 13.

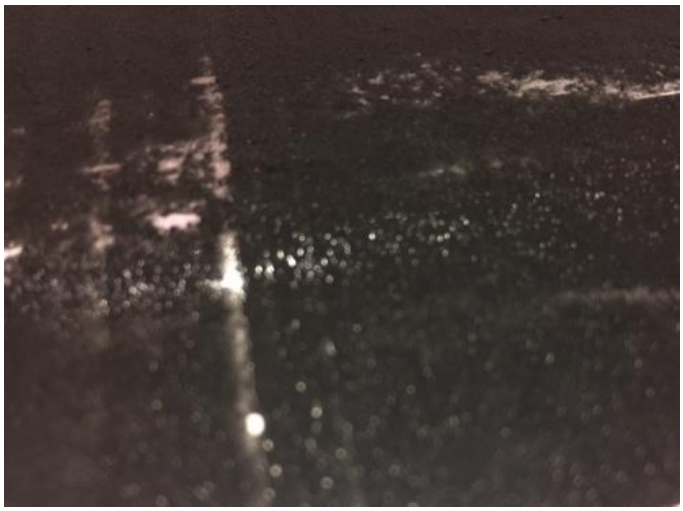

Figure 12: LiPAA:SBR (50:50) Poor Quality Surface Coating

Figure 13: Pure SBR Cathode Degradation

It is hypothesized that this severe degradation is a result of particle agglomeration [25,26], which is the accumulation of particles as a result of high adhesive forces, or side reactions. In this instance, it is likely that the adhesion force of SBR was too high. This is surprising, because SBR was previously found to reduce cracking in anodes [27]. After it was clear that SBR would not in any way reduce the brittle fracture seen in LiPAA cathodes, it was decided to focus all efforts on the LiPAA:Na-Alg combinations instead. SEM images of a cathode with a LiPAA:SBR (50:50) binder ratio were taken and analyzed to quantify the exact severity of surface degradation experienced.

4.1.2 SEM Analysis of Surface Quality

The mechanical analysis on each cathode sample takes the form of SEM imaging. Figures 15 – 21 are shown in order of increasing Na-Alg as a percentage of the overall binder ratio. Each figure is composed of three images. The middle image is from an SEM taken at 100x magnification. It has a red circle highlighting the location of the 250x magnification, which is the rightmost image. The leftmost image is the same as the middle image with higher contrast, and was used for the ImageJ analysis. Figure 15, labeled LiPAA:Na-Alg (100:0), should be read: The cathode which used a 100:0 ratio of LiPAA to Na-Alg as a binder, which itself composes 7.5% of the overall cathode by weight.

In order to establish a baseline, SEM images were also taken of the PVdF cathode shown below in Figure 14. The ImageJ analysis revealed that 4.5% of a PVdF cathode exhibits cracking. It should be noted that this PVdF cathode was created with 200μm thickness rather than a 300μm as the rest of the cathode samples were. This reduces the prominence of the cracking it experiences, and therefore, 4.5% cracking is a conservative estimate compared to what we would expect with a 300μm sample.

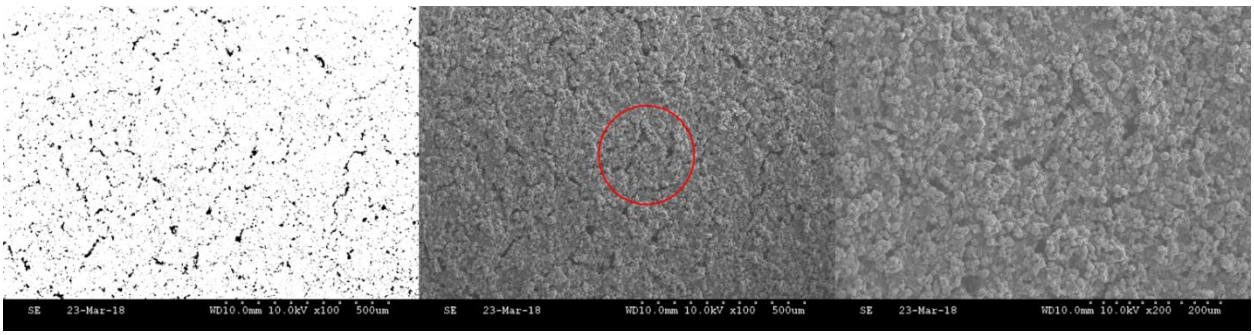

Figure 14: SEM Images of a PVdF Cathode

Figures 15-21 show the SEM and ImageJ images as described above. The percent of these samples that are covered by cracks can be found below in Table 1.

Table 1: Percentage of Cracked Area for each Cathode

Cathode	%Area Cracked
0LiPAA	2.08
30LiPAA	9.26
40LiPAA	5.90
50LiPAA	10.52
60LiPAA	13.76
70LiPAA	14.48
100LiPAA	18.55
50SBR	36.39
PVdF	4.52

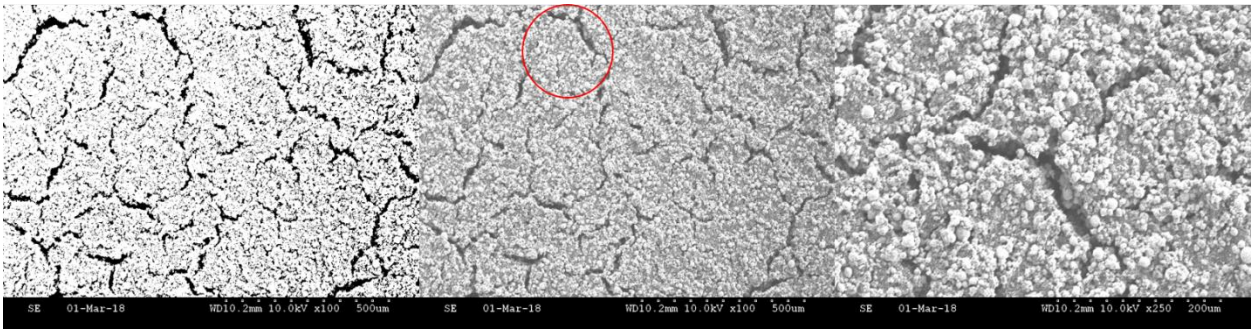

Figure 15: LiPAA:Na-Alg (100:0)

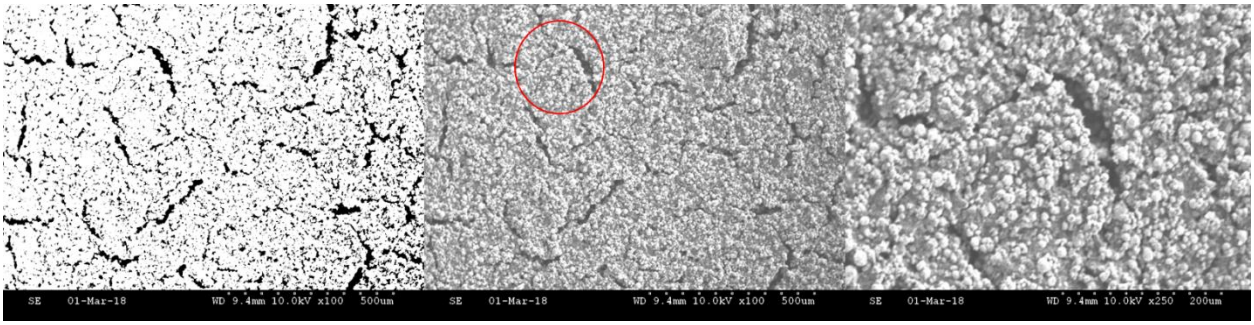

Figure 16: LiPAA:Na-Alg (70:30)

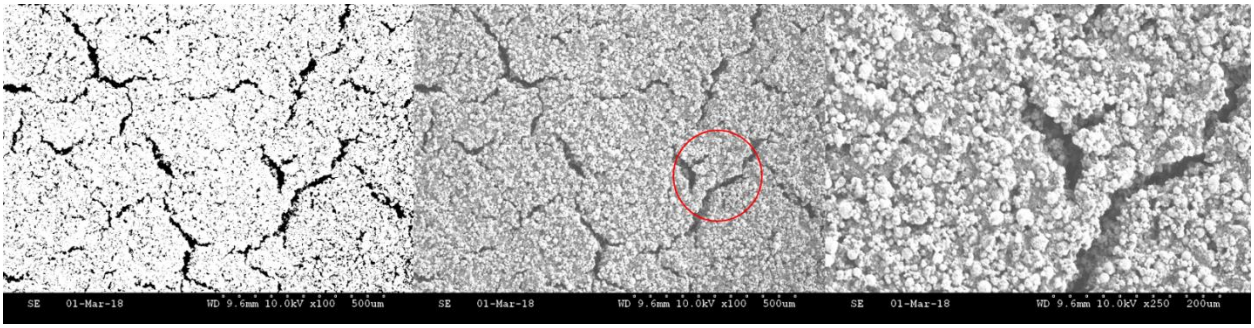

Figure 17: LiPAA:Na-Alg (60:40)

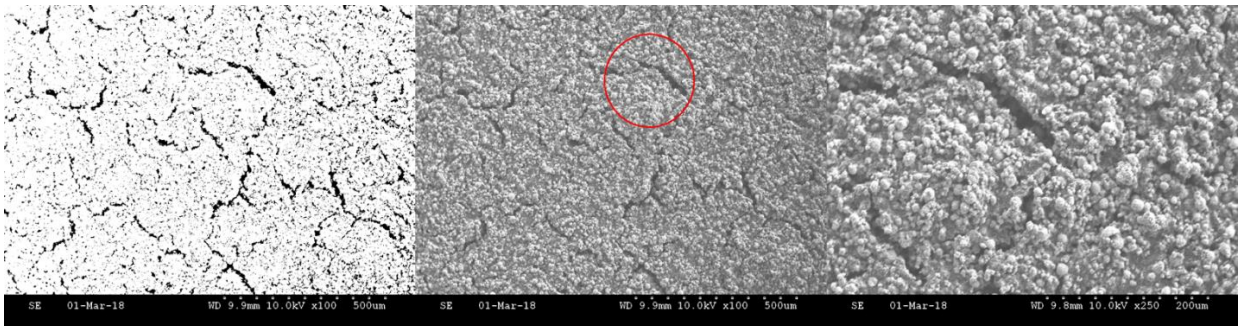

Figure 18: LiPAA:Na-Alg (50:50)

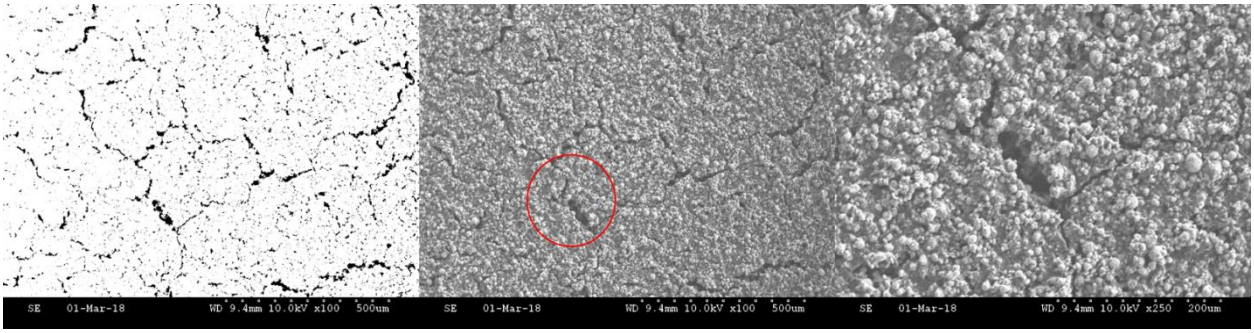

Figure 19: LiPAA:Na-Alg (40:60)

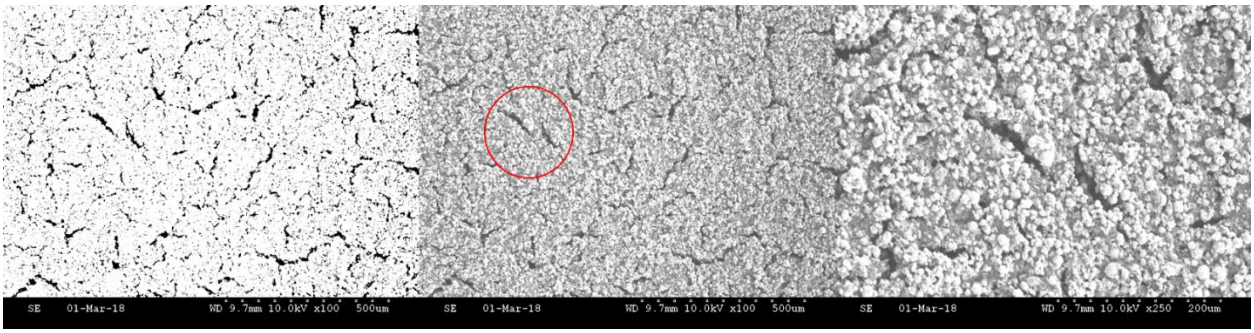

Figure 20: LiPAA:Na-Alg (30:70)

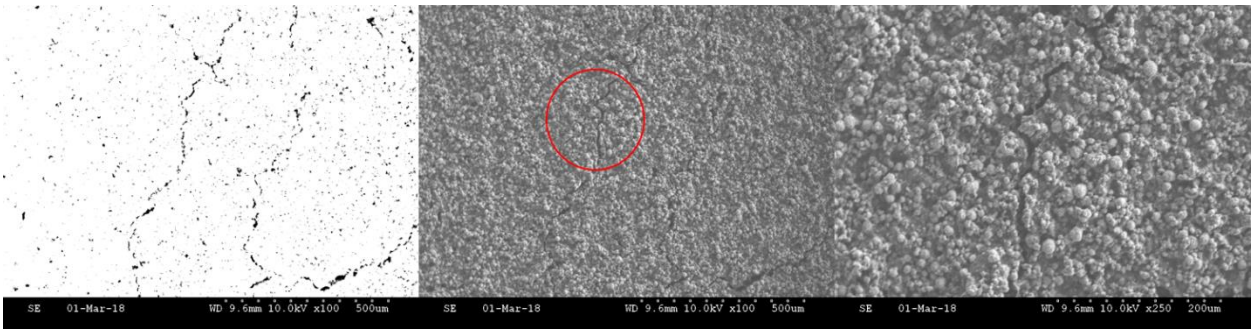

Figure 21: LiPAA:Na-Alg (0:100)

For comparison, Figure 22 below shows the LiPAA:SBR (50:50) cathode. This severe cracking covers more than 36% of the surface, nearly double the 18.5% of the cathode experiencing the second most severe cracking, LiPAA:Na-Alg (100:0).

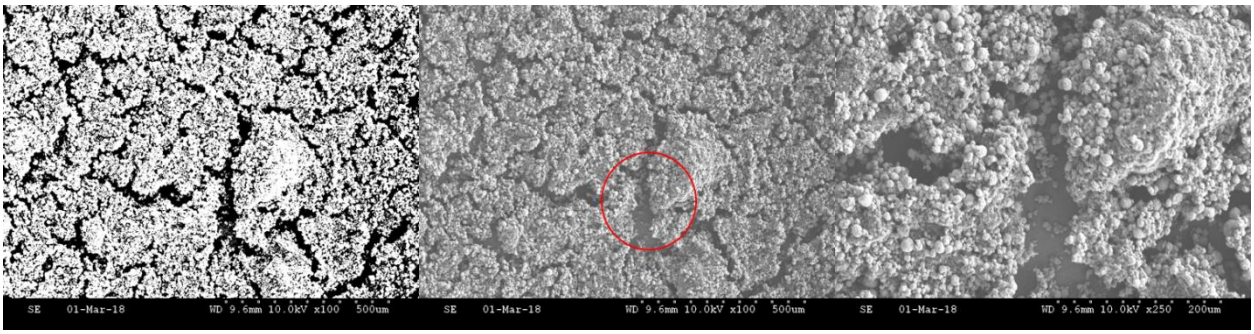

Figure 22: LiPAA:SBR (50:50)

Aside from the LiPAA:Na-Alg (30:70) and LiPAA:Na-Alg (40:60) cathodes, the percent of cracking followed a nearly linear trend as shown in Figure 23 below.

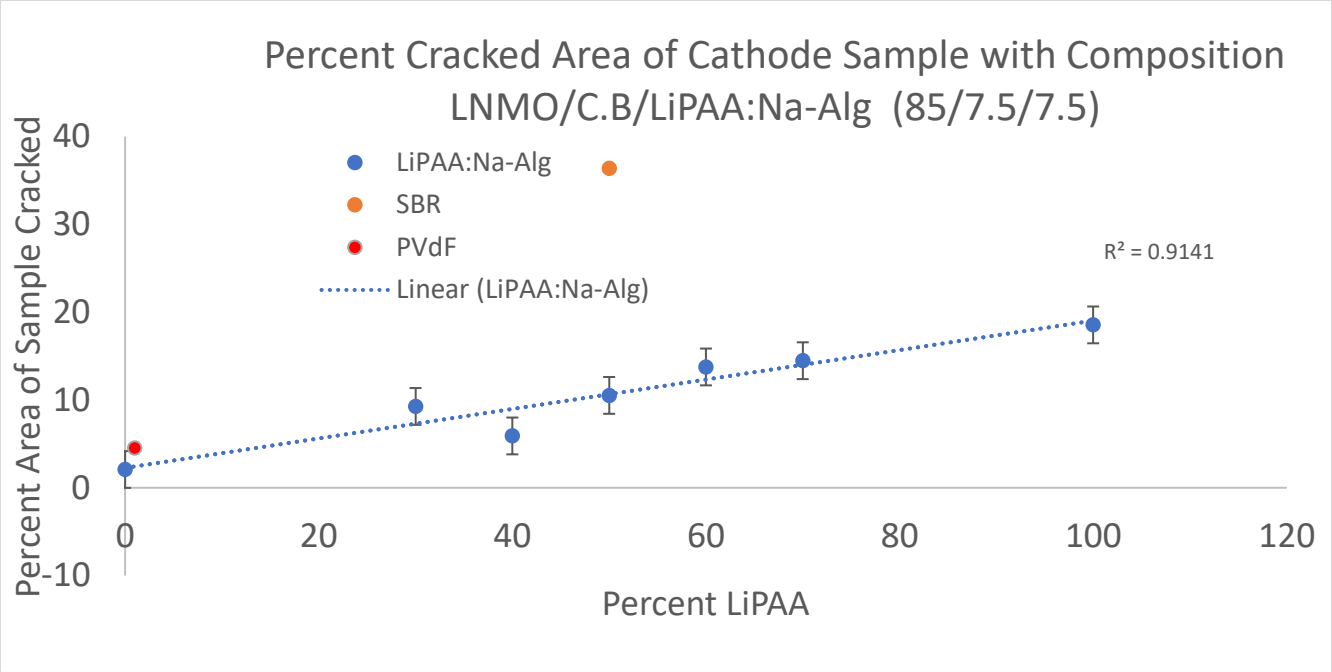

Figure 23: Percent Cracking vs. Percent of Binder composition as LiPAA, with Standard Error Bars

With an R^2 value of .914 and standard error, error bars as shown, the linear fit appears to accurately describe the relationship between the percentage cracking experienced, and the amount of LiPAA in the binder. This shows that adding Na-Alg to LiPAA does indeed reduce the amount of cracking exhibited by the sample, as hypothesized. The SBR cathode, shown in orange, is clearly shown to be far too pulverized to consider it as an effective crack reducer.

In order to determine what level of reduction in cracking is sufficient for commercial use, these cathodes must be compared to the industry standard PVdF cathode. As seen in Table 1, 4.5% of the PVdF cathode sample was covered in cracks. While the maximum cracking that can occur in a cathode for large scale manufacturing is not well defined, it is reasonable to assume that if the cracking is lower that exhibited by the current industry standard, then it can be considered sufficiently low. Based on this assumption, and taking the linear crack reduction trend into consideration, it appears that cathodes using LiPAA:Na-Alg (20:80) will exhibit less

than 4.5% cracking, and thus are suitable for manufacturing. It should be noted that cathodes using a greater ratio of LiPAA to Na-Alg may be viable on a manufacturing scale, however we cannot assume that this is the case based on control data from the PVdF cathode.

4.2 Electrochemical Results

The electrochemical results of this experiment are primarily focused on the overall capacity and capacity fade of the cell. Both half and full cells were created. The results from each of these will be analyzed separately. Half and full cells created using samples from the same cathode batch either failed almost immediately upon cycling or exhibited drastic capacity face, showing that SBR is not a viable binder additive to cathodes utilizing LiPAA. As a result, all reported data is of LiPAA:Na-Alg mixtures.

4.2.1 Half Cell Data

Data obtained using half cells provides a reliable proof of concept for individual materials within the cell that are currently being tested. Though half cells do not experience the full range of side reactions present in a full cell – most notably SEI formation – they provide a streamlined way to observe capacity and cycle life trends.

4.2.1 Capacity Fade Results

Figures 24-30 below, show a discharge capacity graph and a voltage vs capacity graph for all half cells cycled. The voltage vs capacity graphs show the potential difference between the cathode and the lithium metal anode as the cell is charged and discharged. Capacity fade can be seen on the specific capacity axis: each cycle ends with a progressively lower and lower specific capacity. The flatter the profile for the discharge capacity graphs, the lower the capacity fade, and the more reliable the battery. For unknown reasons the half cell containing a PVdF cathode

failed, behaving erratically for the first few cycles before failing. For this reason, the data is not included here.

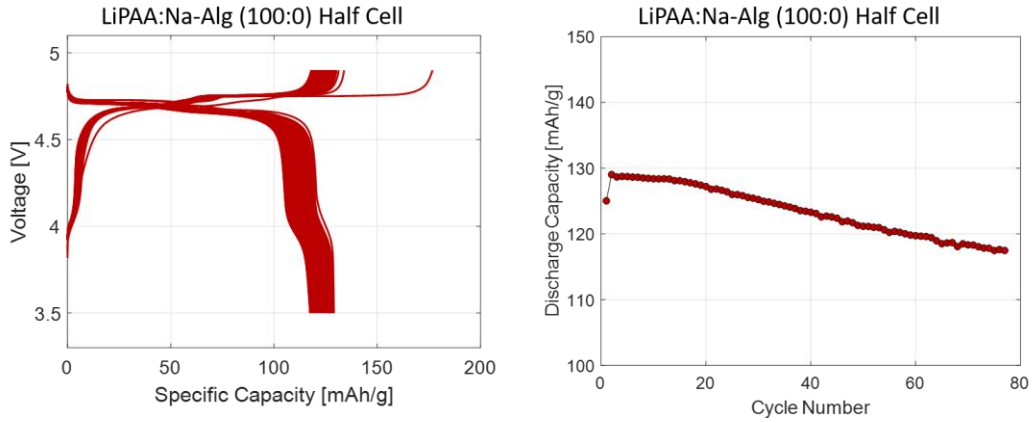

Figure 24: LNMO/C.B./LiPAA:Na-Alg (100:0) Half Cell. Left - Voltage vs Specific Capacity. Right - Discharge Capacity

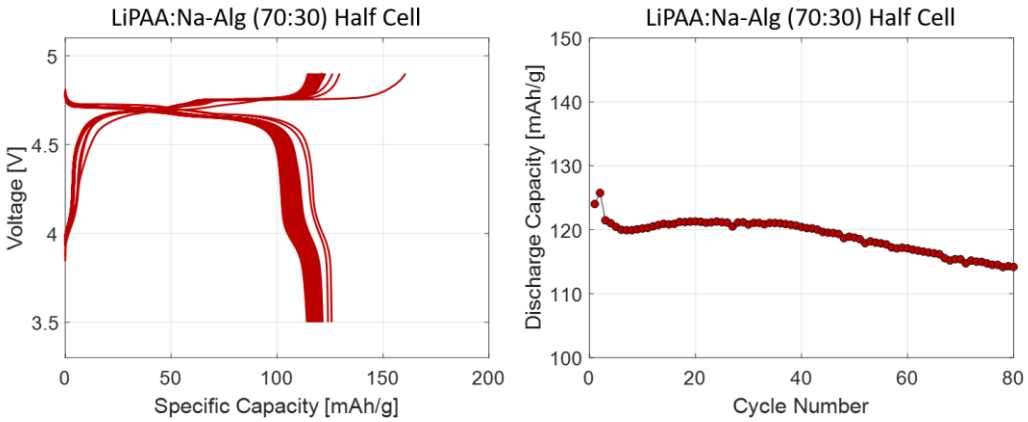

Figure 25: LNMO/C.B./LiPAA:Na-Alg (70:30) Half Cell. Left - Voltage vs Specific Capacity. Right - Discharge Capacity

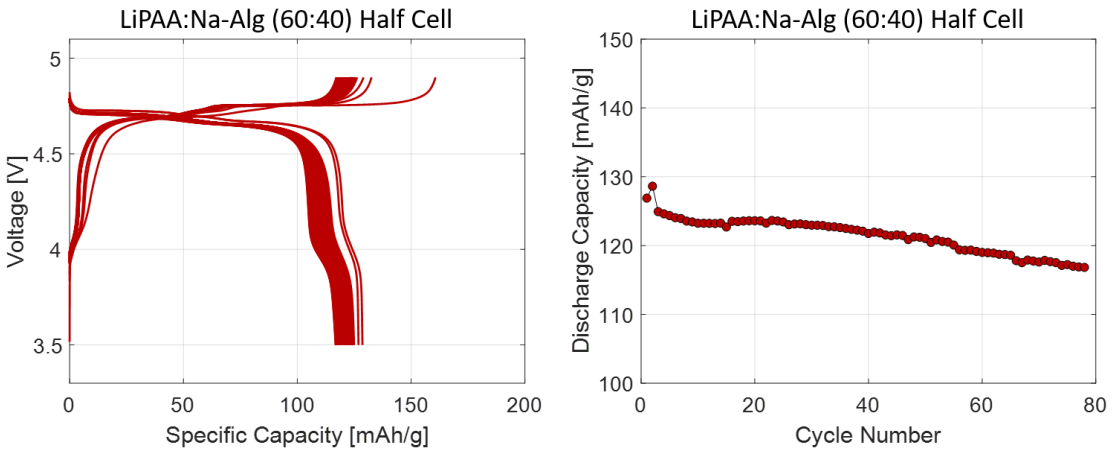

Figure 26: LNMO/C.B./LiPAA:Na-Alg (60:40) Half Cell. Left - Voltage vs Specific Capacity. Right - Discharge Capacity

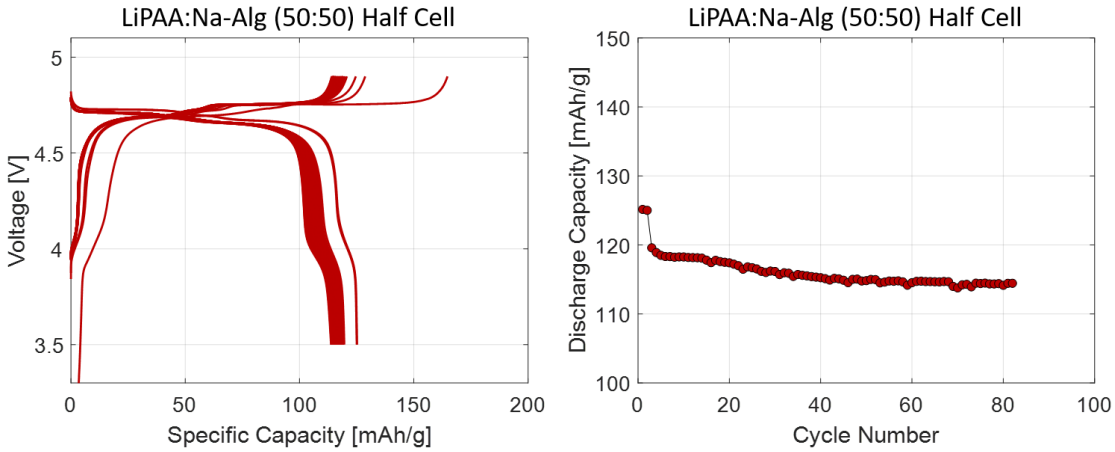

Figure 27: LNMO/C.B./LiPAA:Na-Alg (50:50) Half Cell. Left - Voltage vs Specific Capacity. Right - Discharge Capacity

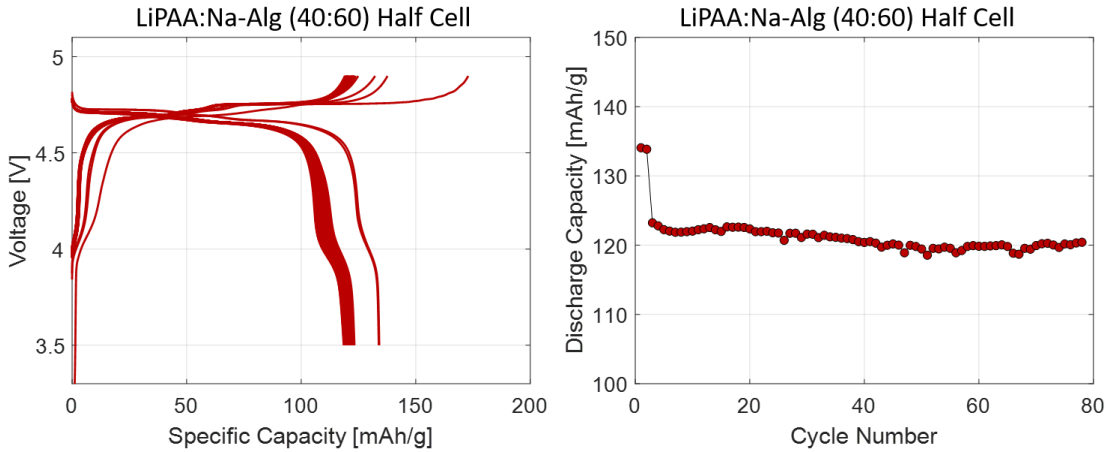

Figure 28: LNMO/C.B./LiPAA:Na-Alg (40:60) Half Cell. Left - Voltage vs Specific Capacity. Right - Discharge Capacity

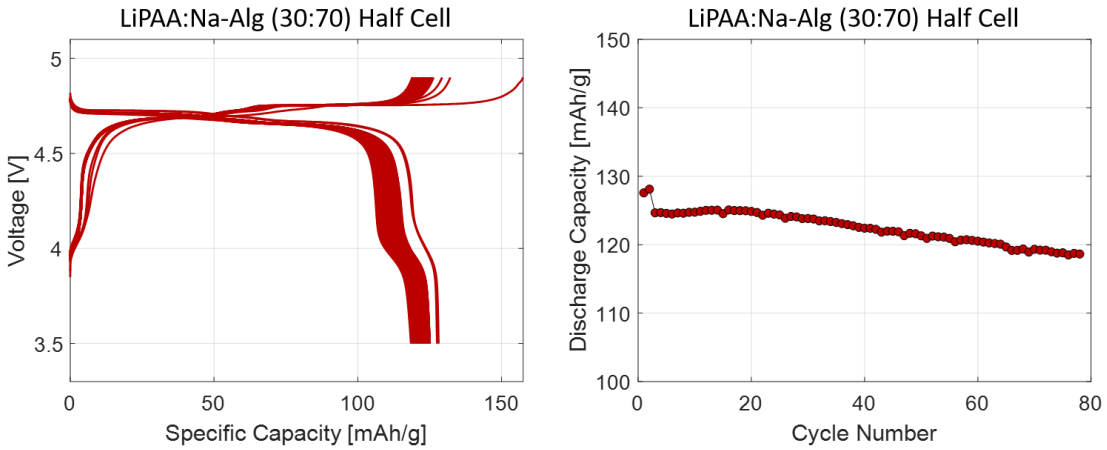

Figure 29: LNMO/C.B./LiPAA:Na-Alg (30:70) Half Cell. Left - Voltage vs Specific Capacity. Right - Discharge Capacity

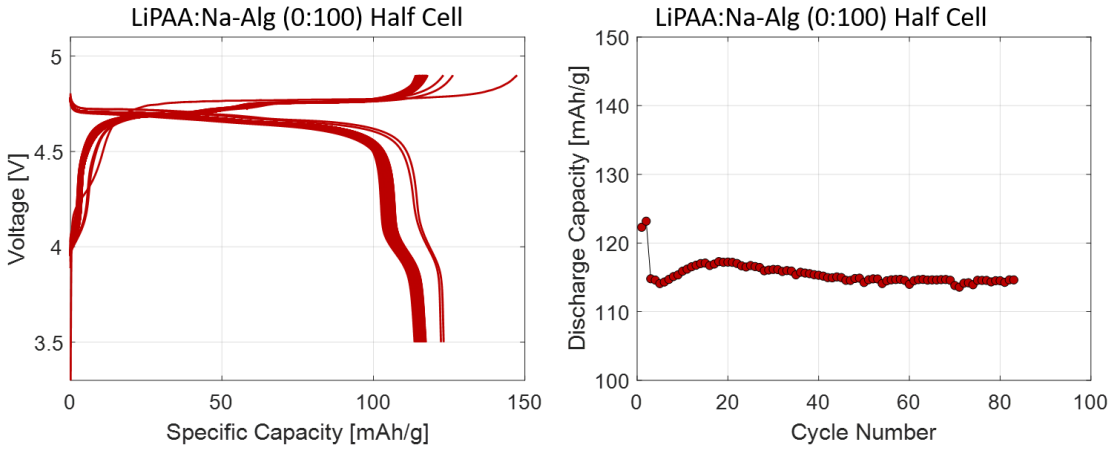

Figure 30: LNMO/C.B./LiPAA:Na-Alg (0:100) Half Cell. Left - Voltage vs Specific Capacity. Right - Discharge Capacity

For comparison the LiPAA:SBR (50:50) half cell is shown below in Figure 31.

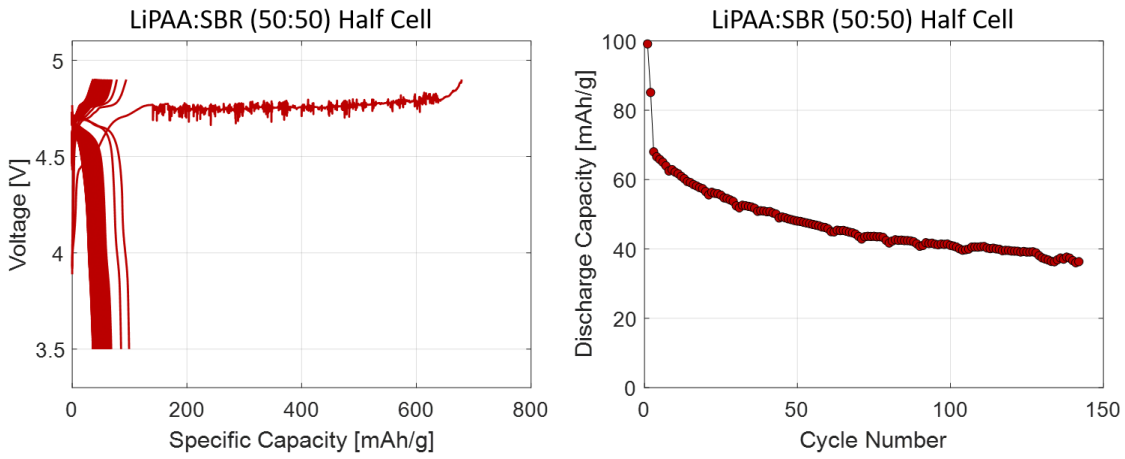

Figure 31: LNMO/C.B./LiPAA:SBR (50:50) Half Cell. Left - Voltage vs Specific Capacity. Right - Discharge Capacity

Table 2 below shows the initial capacity from cycle 3 and percent capacity fade from cycle 3 after 80 cycles for each of the half cells created.

Table 2: Initial Capacity and Capacity Fade for all LiPAA:Na-Alg Half Cells

Half Cell	Initial Capacity (mAh/g)	Percent Capacity Fade After 80 cycles (%)
LiPAA:Na-Alg (100:0)	129	8.5
LiPAA:Na-Alg (70:30)	121	5.2
LiPAA:Na-Alg (60:40)	125	5.6
LiPAA:Na-Alg (50:50)	120	4.1
LiPAA:Na-Alg (40:60)	123	2.4
LiPAA:Na-Alg (30:70)	125	4.8
LiPAA:Na-Alg (0:100)	117	1.7
LiPAA:SBR (50:50)	69	42.0

In order to determine any trends, initial capacity vs percent LiPAA and percent capacity fade vs percent LiPAA are graphed below in Figures 32 and 33 respectively using standard error, error bars.

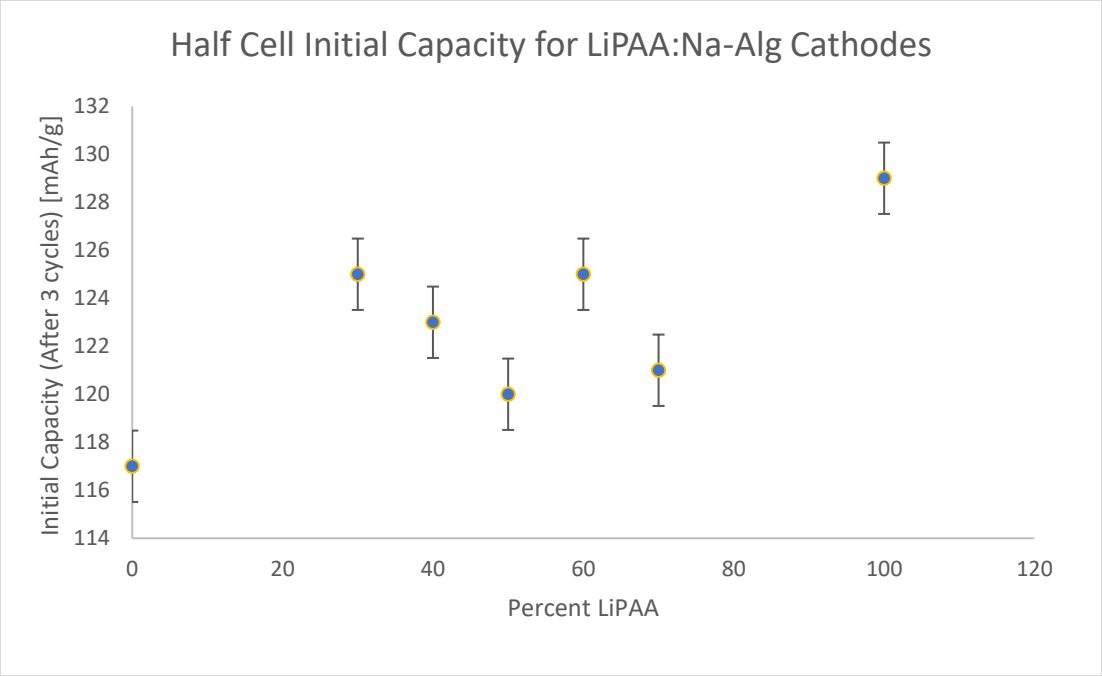

Figure 32: Half Cell Initial Capacity for LNMO/CB/LiPAA:Na-Alg Cathodes

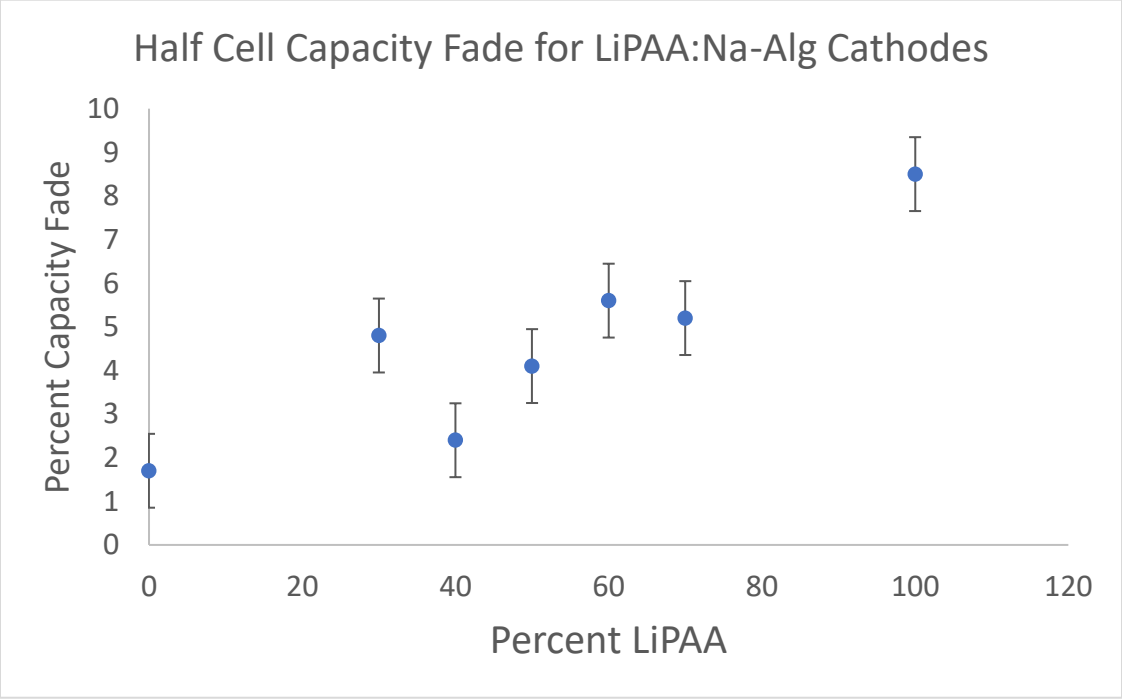

Figure 33: Half Cell Capacity Fade for LNMO/CB/LiPAA:Na-Alg Cathodes

A few things are noteworthy about these figures. First and foremost, they corroborate the idea that LiPAA provides some additional initial capacity to the cell over a pure Na-Alg binder.

The LiPAA:Na-Alg (100:0) half cell had 129 mAh/g of initial capacity, and the LiPAA:Na-Alg (0:100) had 117 mAh/g of initial capacity; a difference of about 9%. The data with mixed binder ratios however, shows only an ambiguous, yet generally upward, trend in the initial capacity as the percent of LiPAA in the binder is increased. With a linear trend R^2 value of .49, and no sign of an exponential trend, the data does not exhibit a strong correlation between initial capacity and percent LiPAA with respect to the binder. A stronger correlation was expected as a result of the donation of Li ions from LiPAA to intercalation. These additional Li ions increased linearly as the percent of LiPAA in the binder was increased so a corresponding linear increase in the initial capacity was anticipated.

The plot of percent capacity fade vs percent LiPAA shows a similarly vague increase in capacity fade as the percentage of LiPAA in the binder was increased. The LiPAA:Na-Alg (100:0) half cell exhibited a 8.5% capacity fade after 80 cycles and the LiPAA:Na-Alg (0:100) half cell exhibited a 1.7% capacity fade after 80 cycles. The pure Na-Alg half cell therefore exhibited about 80% less capacity fade than the pure LiPAA half cell. This significant capacity fade reduction, and can be attributed to a reduction in side reactions with the electrolyte. This was not anticipated however, since LiPAA produces a passivating layer on the cathode to prevent additional side reactions. As before, the data collected for half cells with mixed binder ratios displays a clear upward trend. With a linear trend R^2 value of .79 and the standard error bars shown, this data exhibits a strong correlation between capacity fade, and percent LiPAA in the binder.

4.2.3 Conclusions from Half Cell Data

Since half cells show simplified capacity fade profiles – without the important SEI formation step included – they are only useful for drawing preliminary conclusions and

correlations regarding the effect of LiPAA on capacity fade and overall cycle life. From the half cell data analyzed here we can determine that there is an increase in initial capacity and an increase in capacity fade as the percent of LiPAA in the binder increases. In order to draw specific conclusions about trends for the mixed binders and to quantify these relationships, full cells must be created and analyzed.

4.2.4 Full Cell Data

As stated above, full cell data provides useful insight into the functional properties of a Li-Ion battery cell. Since using Li metal as the anode (which is how half cells are created) is dangerous in scaled up commercial batteries, graphite and other types of anodes are used in its place. These replacement anodes require a SEI) to form in order to protect the anode from scavenging reactions with the electrolyte. SEI formation uses a significant amount of Li reducing the overall capacity of the battery. Additionally, every time the SEI is damaged, more Li is consumed to repair it. This results in significantly higher capacity fade, and lower initial capacity for full cells as compared to half cells. For this reason, full cell data is necessary to quantify the electrochemical effects resulting from subtle differences in cathode composition.

4.2.5 Capacity Fade Results

Figures 34-41 below, show a discharge capacity graph and a voltage vs capacity graph for all full cells cycled. The SBR cathode did not even complete one full cycle before failure so SBR plots are not included. The control PVdF cell is shown first.

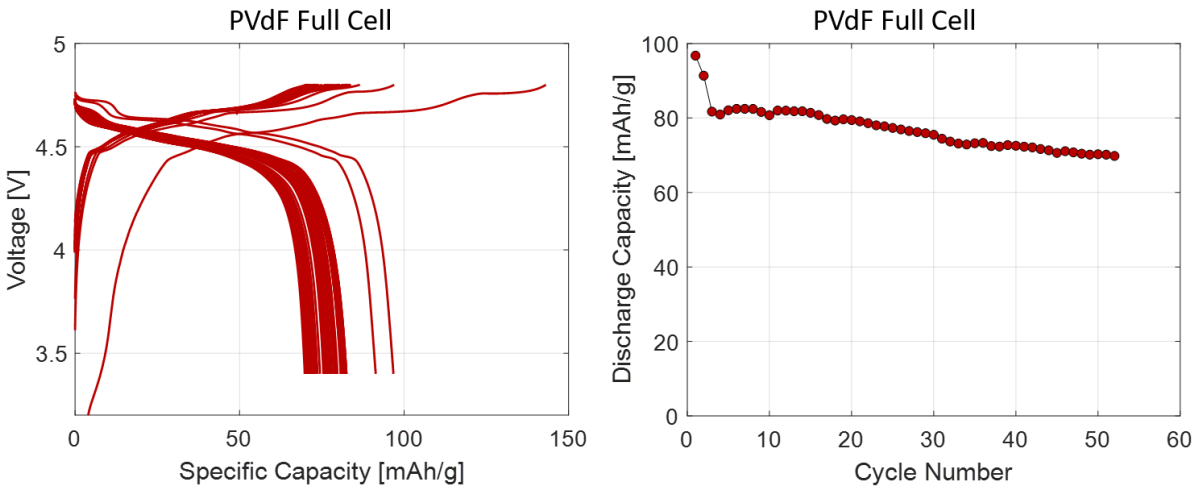

Figure 34: LNMO/C.B./PVdF Full Cell. Left - Voltage vs Specific Capacity. Right - Discharge Capacity

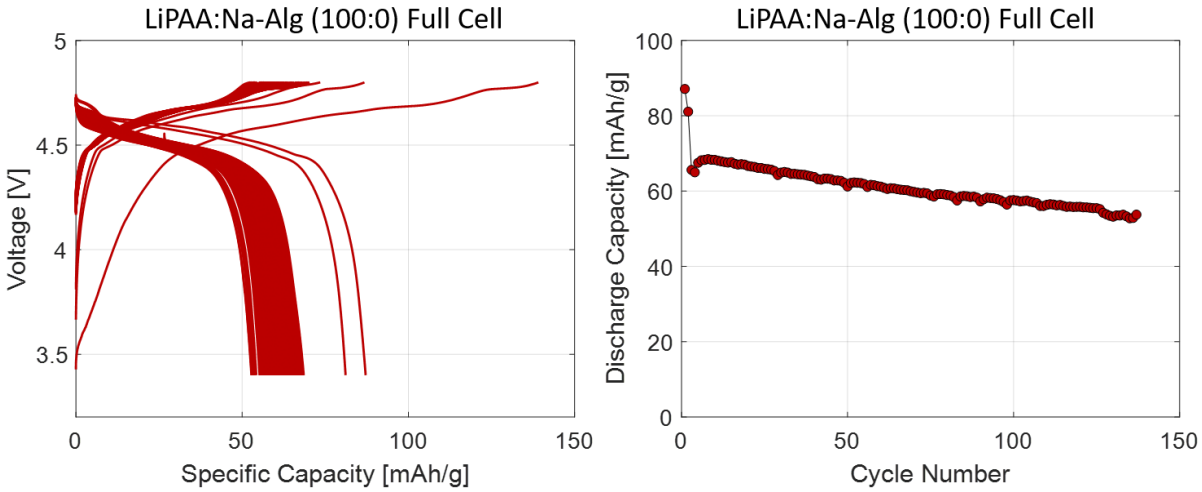

Figure 35: LNMO/C.B./LiPAA:Na-Alg (100:0) Full Cell. Left - Voltage vs Specific Capacity. Right - Discharge Capacity

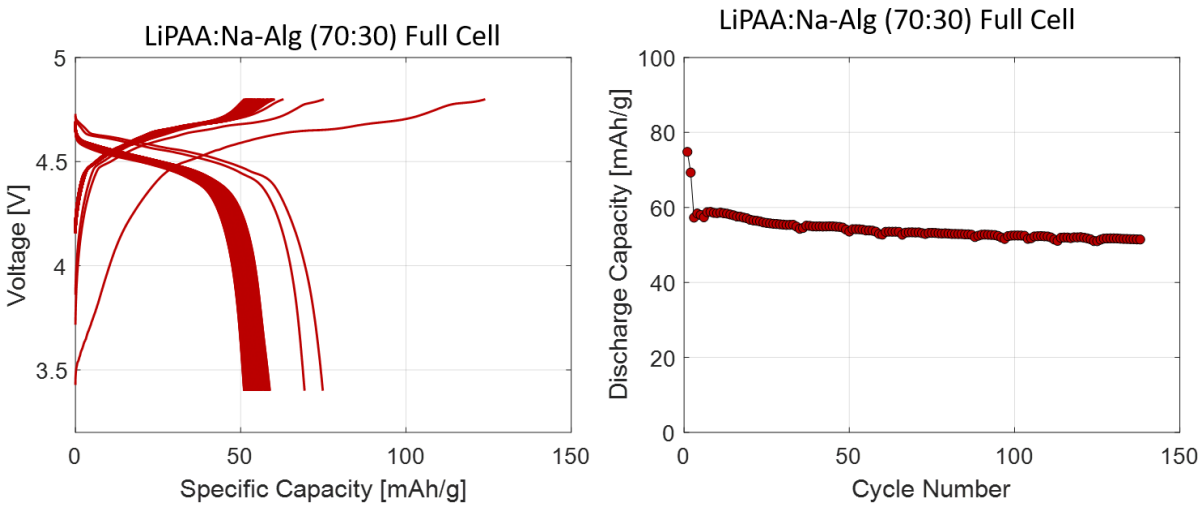

Figure 36: LNMO/C.B./LiPAA:Na-Alg (70:30) Full Cell. Left - Voltage vs Specific Capacity. Right - Discharge Capacity

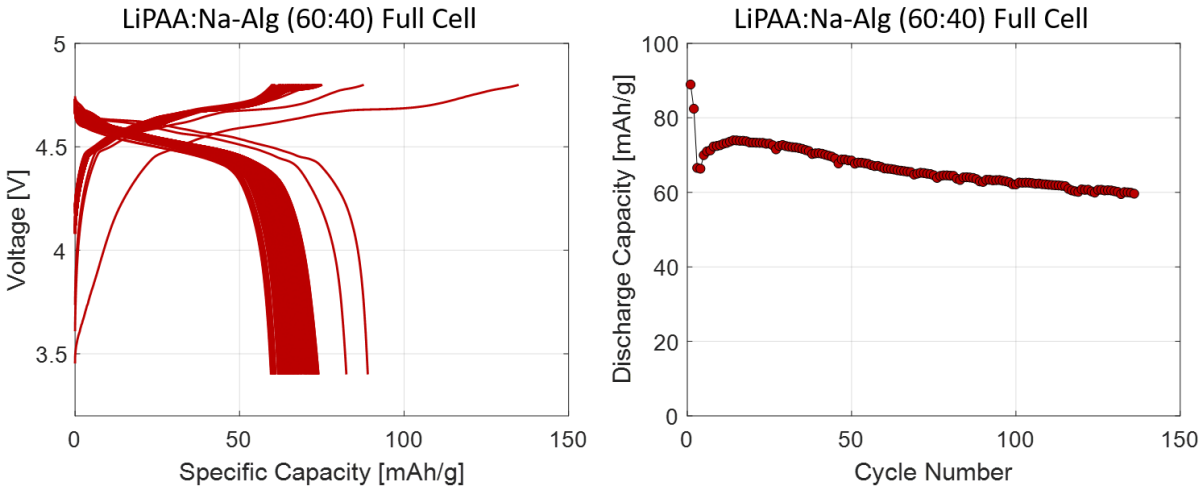

Figure 37: LNMO/C.B./LiPAA:Na-Alg (60:40) Full Cell. Left - Voltage vs Specific Capacity. Right - Discharge Capacity

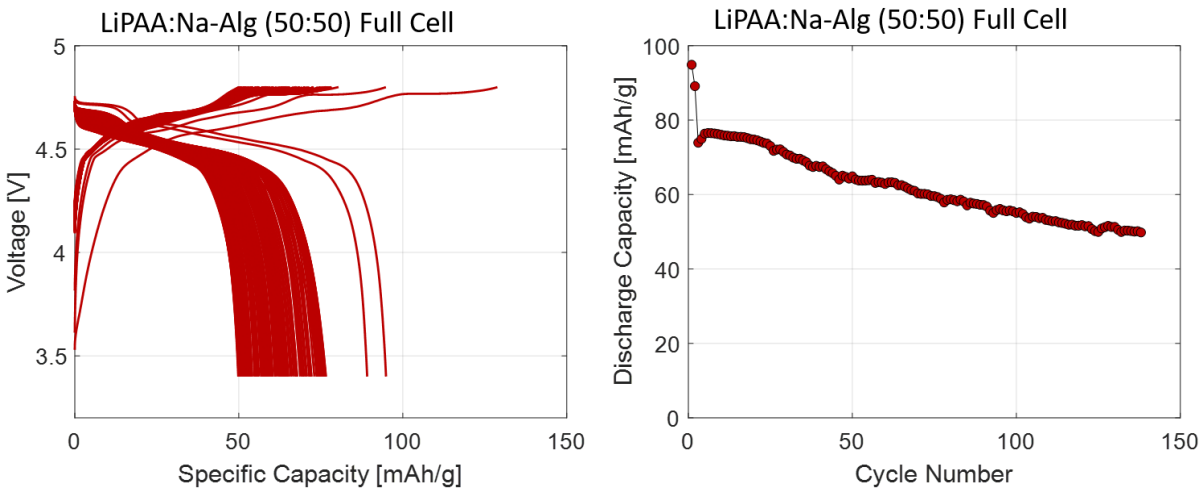

Figure 38: LNMO/C.B./LiPAA:Na-Alg (50:50) Full Cell. Left - Voltage vs Specific Capacity. Right - Discharge Capacity

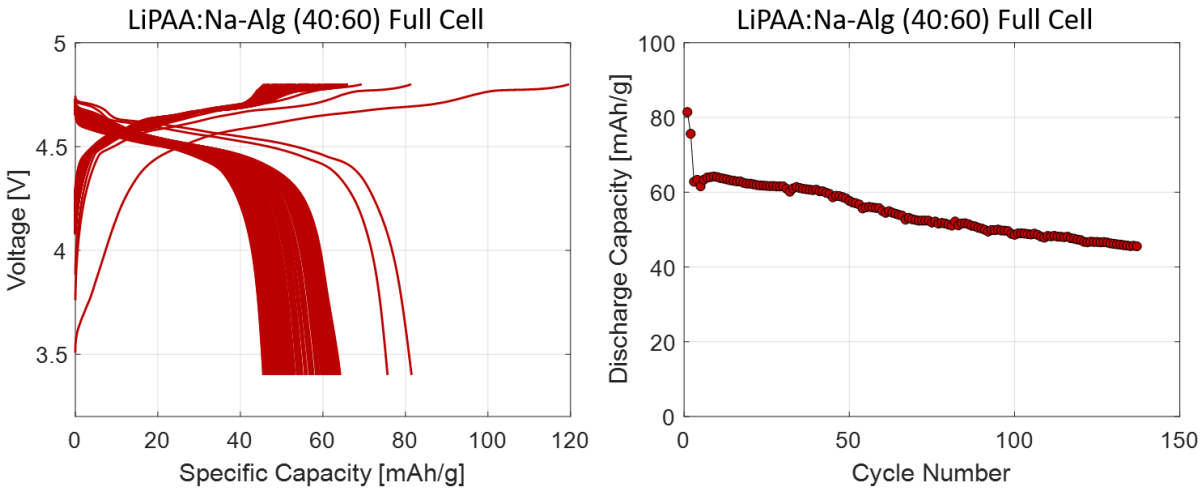

Figure 39: LNMO/C.B./LiPAA:Na-Alg (40:60) Full Cell. Left - Voltage vs Specific Capacity. Right - Discharge Capacity

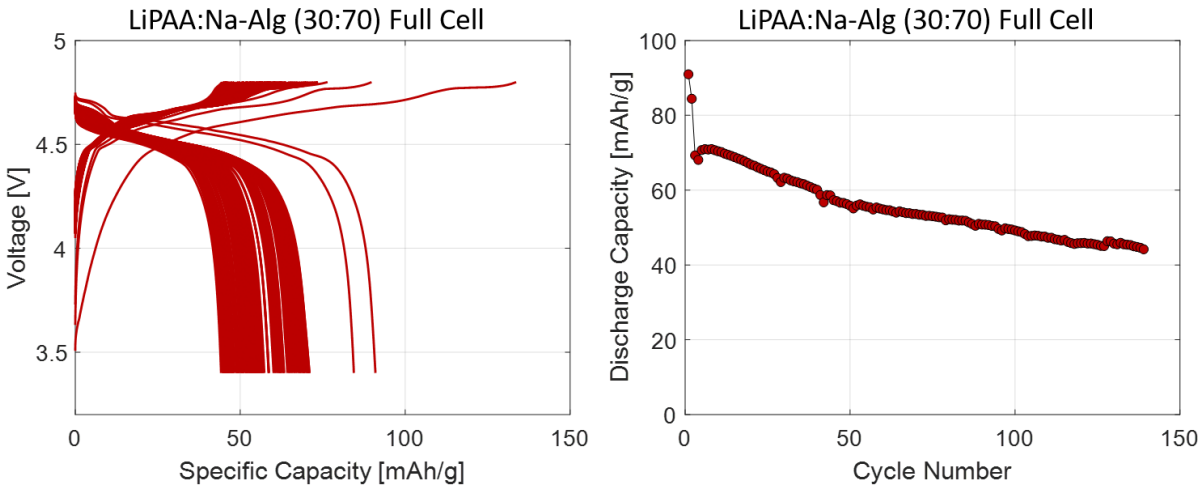

Figure 40: LNMO/C.B./LiPAA:Na-Alg (30:70) Full Cell. Left - Voltage vs Specific Capacity. Right - Discharge Capacity

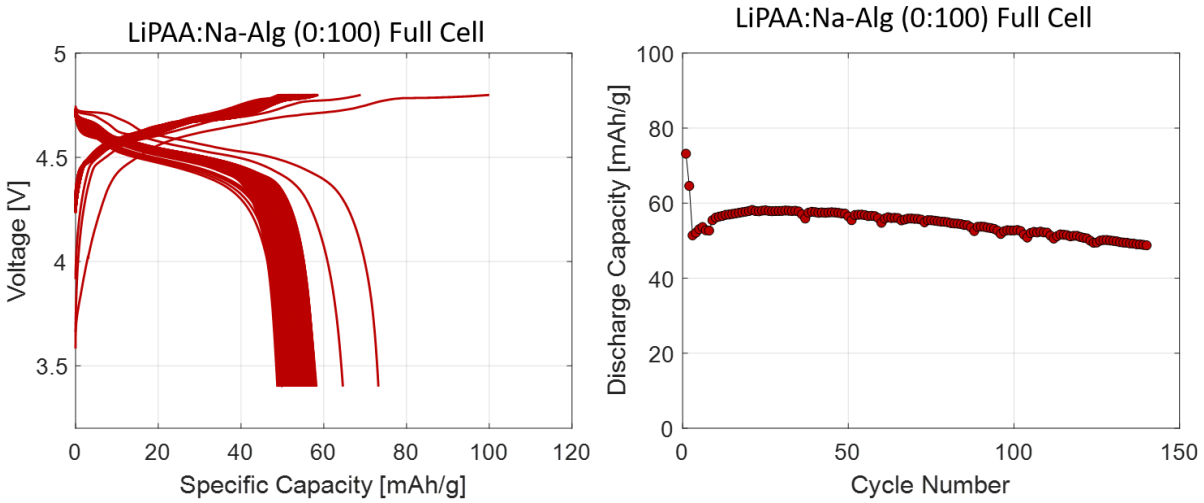

Figure 41: LNMO/C.B./LiPAA:Na-Alg (0:100) Full Cell. Left - Voltage vs Specific Capacity. Right - Discharge Capacity

Table 3 shows the initial capacity from cycle 5 and percent capacity fade from cycle 5 after 80 cycles for each of the full cells created (PVdF is shown for 40 cycles).

Table 3: Initial Capacity and Percent Capacity Fade for Full Cells

Full Cell	Initial Capacity (mAh/g)	Percent Capacity Fade After 50 cycles (%)	Percent Capacity Fade After 125 cycles (%)
LiPAA:Na-Alg (100:0)	66	7.5	16.7
LiPAA:Na-Alg (70:30)	59	6.8	11.8
LiPAA:Na-Alg (60:40)	75	7.1	20
LiPAA:Na-Alg (50:50)	77	18.2	35.1
LiPAA:Na-Alg (40:60)	62	4.8	29
LiPAA:Na-Alg (30:70)	72	22.2	40.3
LiPAA:Na-Alg (0:100)	16.9	1.6	16.9
LiPAA:SBR (50:50)	N/A	41.1	N/A
PVdF	80	12.5	N/A

In order to determine any trends, initial capacity vs percent LiPAA and percent capacity fade vs percent LiPAA are graphed in Figures 42 and 43 respectively.

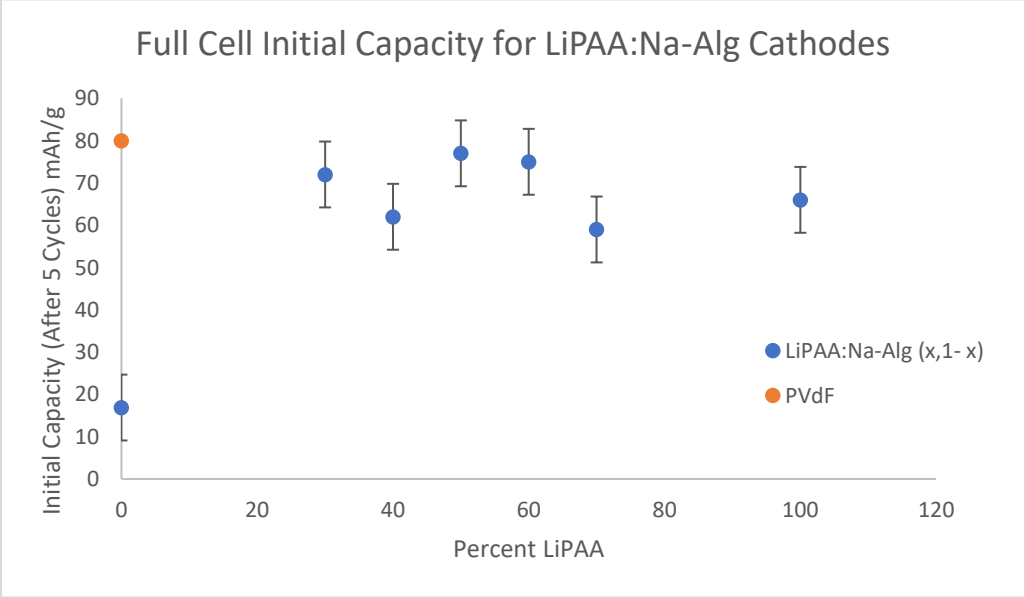

Figure 42: Full Cell Initial Capacity for LNMO/CB/LiPAA:Na-Alg Cathodes

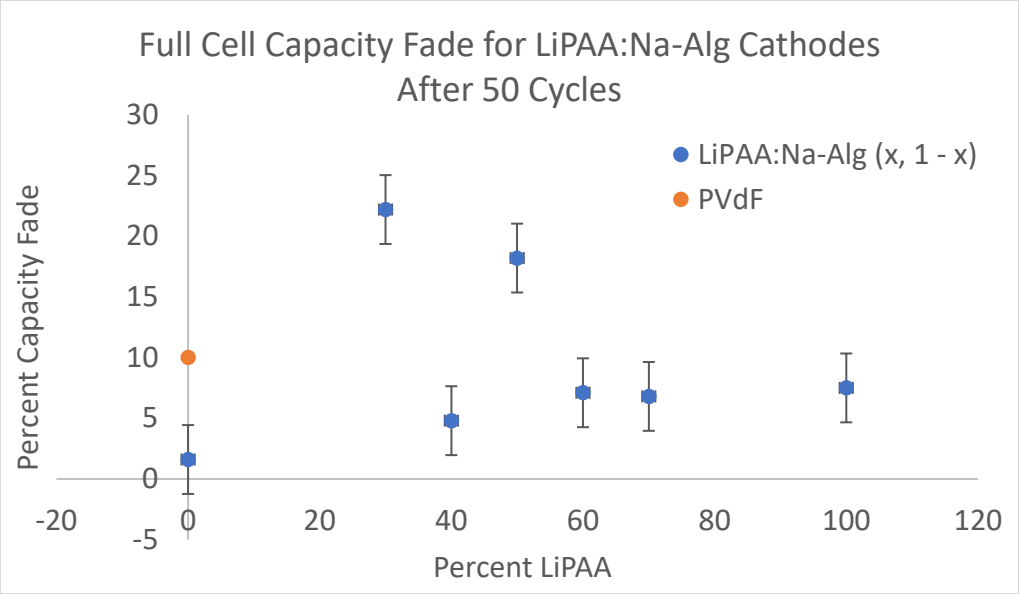

Figure 43: Full Cell Capacity Fade for LNMO/CB/LiPAA:Na-Alg Cathodes

It is immediately noticeable that the initial specific capacity is much lower for each full cell than for the half cells analyzed previously. The full cell with the highest initial capacity was PVdF with 80 mAh/g, more than half as low as the 129 mAh/g the LiPAA:Na-Alg (100:0) half cell exhibited. This is a result of the SEI generation, as discussed previously. It is also noteworthy that the PVdF full cell had a higher initial capacity than all LiPAA:Na-Alg cells. As mentioned several times already, the lithium in the LiPAA binder is supposedly lithiated along with the other lithium ions in the cathode during charging which should result in excess capacity when compared the PVdF cell. Though some cells, namely LiPAA:Na-Alg (50:50) with 77 mAh/g, had a comparable initial capacity to PVdF, the fact that PVdF had the highest initial capacity puts forth evidence that LiPAA does not provide additional capacity to the battery. Further, there is no clear trend in the data regarding an increase in initial capacity as percent LiPAA increases, even when only considering the LiPAA:Na-Alg samples.

Looking at capacity fade, a slightly different story emerges. The PVdF full cell exhibits 12.5% capacity fade over 50 cycles, where the LiPAA:Na-Alg (100:0) full cell exhibits only 7.5% capacity fade over 50 cycles, and only 16.7% capacity fade over 125 cycles. This clearly shows that LiPAA provides some measure of capacity fade reduction compared to PVdF, about 40% in fact which is in line with findings of Kim and others [9]. The pure Na-Alg sample exhibited relatively low (1.6%) capacity fade over 50 cycles, but 16.9% capacity fade after 125 cycles. Setting aside this sample, a clear downward, if not quite linear, trend emerges with the rest of the data. Increasing percent LiPAA in the binder results in a decreased percent capacity fade. No immediate trend appears in this data when looking at the graph. However, when factoring in the 125-cycle data, it appears that increasing the percentage of Na-Alg in the binder generally increases the amount of capacity fade experienced. This was expected in that the lithium ions present in the LiPAA are donated to compensate for scavenging reactions between the transported lithium and electrolyte. It makes sense that reducing the LiPAA in the binder (by adding Na-Alg) would reduce this benefit, though the extent of degradation is perhaps a bit surprising. This shows that the cathode and coin cell creation process were not fully optimized for these chemistries.

4.2.6 Conclusions from Full Cell Data

After analyzing the full cell data it is clear that the additional lithium ions that are being provided through the use of LiPAA as a binder reduce the capacity fade of the cell rather than increasing the initial capacity. This aligns with the data collected by [9], but adds to it by showing that the capacity fade decreases with an increasing percentage of LiPAA. Individual variation in capacity fade makes it difficult to an exact correlation, however, the trend is clear that adding addition LiPAA reduces the amount of capacity fade experienced.

4.3 Conclusions from Mechanical and Electrochemical Data

Considering both the mechanical and electrochemical data, the percent of LiPAA in the binder can be optimized to provide maximum benefits from LiPAA, while reducing cathode pulverization to an acceptable level. From the SEM analysis, and Figure 23 in particular, it appears that a conservative maximum percentage of LiPAA in the binder is 20%, with the remaining 80% as Na-Alg. Though this is a lower than desired percentage of LiPAA, it will certainly confer some of its initial benefits, especially water solubility and cathode passivation layer formation. Looking at the full cell percent capacity fade values in Table 3 shows that increasing the percent of Na-Alg significantly increases the capacity fade experienced by the cell. From the limited data set available, it appears that lowering the LiPAA present in the binder enough to sufficiently reduce the brittle fracture experienced, would also increase the capacity fade to greater than 40% after 125 cycles, which is astronomically high. Though Na-Alg does indeed reduce the cracking exhibited by LiPAA cathodes in a predictable way, further optimization of the cathode and overall process are required in order to determine the optimum ratio of LiPAA:Na-Alg, such that cracking is sufficiently reduced, and capacity fade is sufficiently low.

Chapter 5: Conclusion

The purpose of this project was to improve the mechanical integrity of cathodes that use LiPAA as a binder, while retaining LiPAA's desirable electrochemical properties.

5.1 Contributions

Li-Ion batteries are used in a wide variety of portable electronic products and power storage systems from cell phones, to medical devices, to EVs, to storage for renewable power generation and everything in between. In order to ensure that these products can continue to improve while also increasing the safety and environmental friendliness of the batteries they contain, it is important to research Li-ion battery materials that further the goals of increased energy density, reduced cost and reduced environmental impact.

The findings of this research help to flesh out the information currently available for LiPAA as cathode binder, a material which not only reduces the cost of Li-ion batteries by about 12.5%, but does it in a way that decreases capacity fade, and reduces reliance on toxic materials such as NMP. This research shows that LiPAA can become more viable when doped with Na-Alg, because the cracking – which pure LiPAA cathodes are prone to – is significantly reduced by Na-Alg. This discovery facilitates further research into LiPAA as a binder for cathodes, speeding up its adoption, and bestowing its benefits onto manufacturers and consumers alike.

5.2 Future Work

Perhaps the most exciting result from this research is its capacity to spur further work in the field of LiPAA cathode research. Since LiPAA provides a passivating layer over the cathode protecting against side reactions with the electrolyte outside of the voltage window, this research opens up the possibility to test new high voltage cathodes that were previously inaccessible such as $LiNiPO_4$, $LiCu_{0.5}Mn_{1.5}O_4$, and $LiNiVO_4$ among others [28]. Since LiPAA has been tested in this research with LNMO, a next step to take would be testing it with a different high voltage

cathode, and studying the effects of the passivating layer on preventing side reactions between the cathode and the electrolyte.

The water solubility of LiPAA, contrasting with the reactivity of NMP with even atmospheric moisture, opens up new avenues of research for Li-Ion battery manufacturing facilities. Specifically, with batteries using LiPAA and water as the binder and solvent respectively, there is no need to worry about how the humidity, which varies depending on the weather, affects the quality of the cathode. Removing this constraint allows space for new innovation in a manufacturing setting.

5.3 Summary

The effects of Na-Alg on the brittle fracture of cathodes utilizing LiPAA as a binder in Li-ion batteries has been studied. It was determined that increasing the percentage of Na-Alg in the binder linearly reduces the cracking experienced by the cathode. Upon cycling these samples, it was shown that increasing the percentage of LiPAA in the cathode generally decreases the capacity fade experienced by the full cell, resulting in longer battery life. The cathodes were created at Nanotech West and coins cells were fabricated at Center for Automotive Research West on OSU's west campus. These findings add to the limited current body of research concerning LiPAA as a cathode binder. The reduction in crack density shown in these results will continue to drive research into LiPAA and its uses in high voltage cathodes.

Appendix A: Electrode Creation Data

Table 4: Cathode Creation Data

Date	Binder Composition	Weight LNMO (g)	weight C.B. (g)	Weight Binder (g)	mass/volume of solvent added (g or mL)	Height of Dr. Blade (um)	Vacuum time (min)	Total Weight (g)	Active Material Percent
1/15/2018	LiPAA	1.7007	0.1483	1.4938	4 mL	600	0	1.9984	0.851
1/15/2018	Na-Alg	1.7022	0.1483	0.1496	7 mL	1200	0	2.0001	0.851
1/26/2018	LiPAA	1.6911	0.1510	1.5032	4 mL	200	2.5	1.9924	0.849
1/26/2018	Na-Alg	0.8500	0.0750	0.0766	5 mL	200	2.5	1.0016	0.849
2/2/2018	SBR	1.4999	0.1319	0.2538	4.5113 g	600	2.5	1.7587	0.853
2/2/2018	SBR	1.5042	0.1332	0.2693	4.6687 g	600	2.5	1.7721	0.849
2/4/2018	LiPAA:Na-Alg (1:1)	1.5036	0.1327	LiPAA: 0.6415 Na-Alg 0.0673	2.9291 g	300	2.5	1.7678	0.851
2/8/2018	LiPAA:SBR (1:1)	1.5011	0.1326	LiPAA: 0.6583 SBR: 0.1328	4.3468 g	300	2.5	1.8323	0.819
2/8/2018	SBR:Na-Alg (1:1)	1.5011	0.1368	SBR: 0.1312 Na-Alg 0.0651	5.2532 g	300	2.5	1.7694	0.848
2/24/2018	LiPAA:Na-Alg (50:50)	0.8509	0.0755	2.0026	0.0759 g	300	2.5	1.0015	0.850
2/24/2018	LiPAA:Na-Alg (70:30)	0.8504	0.0757	2.0010	0.0782 g	300	2.5	1.0011	0.849
2/25/2018	LiPAA:Na-Alg (30:70)	0.8498	0.0754	1.9578	0.0784 g	300	2.5	0.9992	0.850
2/25/2018	LiPAA:Na-Alg (60:40)	0.8505	0.0755	2.0026	0.0768 g	300	2.5	1.0011	0.850
2/25/2018	LiPAA:Na-Alg (40:60)	0.8500	0.0760	2.0037	0.0727 g	300	2.5	1.0013	0.849
3/1/2018	LiPAA	0.8502	0.0758	0.7527	1.3259 g	300	2.5	1.0013	0.849

Table 5: Cathode Sample Weight. Highlighted Samples were Paired with Corresponding Highlighted Anode Samples in Full Cells

Cathode Sample	Total Mass (mg)	Mass of Al Foil (mg)	Mass of Cathode (mg)	Mass of Active Material (mg)	Diameter of Sample (mm)	mAh	mAh test	mg Anode
LiPAA 1/15/18	19.9	5.935	13.965	11.9	13.7	1.66	1.60	5.38
LiPAA 1/15/18	29.5	5.935	23.565	20.1	13.7	2.81	2.71	9.08
LiPAA 1/15/18	27.6	5.935	21.665	18.4	13.7	2.58	2.49	8.35
LiPAA 1/15/18	21.6	5.935	15.665	13.3	13.7	1.87	1.80	6.04
Na-Alg 1/15/18	35.4	5.935	29.465	25.1	13.7	3.51	3.39	11.36

Na-Alg 1/15/18	36.4	5.935	30.465	25.9	13.7	3.63	3.50	11.74
Na-Alg 1/15/18	39.0	5.935	33.065	28.1	13.7	3.94	3.80	12.75
Na-Alg 1/15/18	39.7	5.935	33.765	28.7	13.7	4.02	3.88	13.02
LiPAA 1/19/18	40.7	5.935	34.765	29.6	13.7	4.14	3.99	13.38
LiPAA 1/19/18	38.1	5.935	32.165	27.3	13.7	3.83	3.69	12.38
LiPAA 1/19/18	35.3	5.935	29.365	25.0	13.7	3.49	3.37	11.31
LiPAA 1/19/18	33.5	5.935	27.565	23.4	13.7	3.28	3.16	10.61
LiPAA 1/26/18	11.6	5.935	5.665	4.8	13.7	0.67	0.65	2.18
LiPAA 1/26/18	11.3	5.935	5.365	4.6	13.7	0.64	0.61	2.06
LiPAA 1/26/18	12.0	5.935	6.065	5.1	13.7	0.72	0.69	2.33
LiPAA 1/26/18	11.1	5.935	5.165	4.4	13.7	0.61	0.59	1.99
Na-Alg 1/26/18	11.0	5.935	5.065	4.3	13.7	0.60	0.58	1.95
Na-Alg 1/26/18	12.6	5.935	6.665	5.7	13.7	0.79	0.76	2.56
Na-Alg 1/26/18	11.1	5.935	5.165	4.4	13.7	0.61	0.59	1.99
Na-Alg 1/26/18	12.3	5.935	6.365	5.4	13.7	0.76	0.73	2.45
SBR #1 2/2/18	25.6	5.935	19.665	16.8	13.7	2.35	2.26	7.60
SBR #1 2/2/18	33.0	5.935	27.065	23.1	13.7	3.23	3.12	10.45
SBR #1 2/2/18	25.0	5.935	19.065	16.3	13.7	2.28	2.20	7.36
SBR #1 2/2/18	13.7	5.935	7.765	6.6	13.7	0.93	0.89	3.00
SBR #2 2/2/18	21.2	5.935	15.265	13.0	13.7	1.81	1.75	5.87
SBR #2 2/2/18	19.7	5.935	13.765	11.7	13.7	1.64	1.58	5.29
SBR #2 2/2/18	15.0	5.935	9.065	7.7	13.7	1.08	1.04	3.49
SBR #2 2/2/18	21.8	5.935	15.865	13.5	13.7	1.89	1.82	6.10
LiPAA:Na-Alg (1:1) 2/4/18	18.6	5.935	12.665	10.8	13.7	1.51	1.45	4.88
LiPAA:Na-Alg (1:1) 2/4/18	18.4	5.935	12.465	10.6	13.7	1.48	1.43	4.80
LiPAA:Na-Alg (1:1) 2/4/18	19.1	5.935	13.165	11.2	13.7	1.57	1.51	5.07
LiPAA:Na-Alg (1:1) 2/4/18	17.8	5.935	11.865	10.1	13.7	1.41	1.36	4.57
LiPAA:SBR (1:1) 2/8/18	16.6	5.935	10.665	8.7	13.7	1.22	1.18	3.96
LiPAA:SBR (1:1) 2/8/18	14.5	5.935	8.565	7.0	13.7	0.98	0.95	3.18
LiPAA:SBR (1:1) 2/8/18	15.1	5.935	9.165	7.5	13.7	1.05	1.01	3.40

LiPAA:SBR (1:1) 2/8/18	15.6	5.935	9.665	7.9	13.7	1.11	1.07	3.59
SBR:Na-Alg (1:1) 2/8/18	15.2	5.935	9.265	7.9	13.7	1.10	1.06	3.56
SBR:Na-Alg (1:1) 2/8/18	15.9	5.935	9.965	8.5	13.7	1.18	1.14	3.83
SBR:Na-Alg (1:1) 2/8/18	14.6	5.935	8.665	7.4	13.7	1.03	0.99	3.33
SBR:Na-Alg (1:1) 2/8/18	15.4	5.935	9.465	8.0	13.7	1.12	1.08	3.64
LiPAA:Na-Alg (50:50) 2/24/18	21.0	5.935	15.065	12.8	13.7	1.79	1.73	5.80
LiPAA:Na-Alg (50:50) 2/24/18	20.0	5.935	14.065	12.0	13.7	1.67	1.61	5.41
LiPAA:Na-Alg (50:50) 2/24/18	18.8	5.935	12.865	10.9	13.7	1.53	1.48	4.95
LiPAA:Na-Alg (50:50) 2/24/18	19.6	5.935	13.665	11.6	13.7	1.63	1.57	5.26
LiPAA:Na-Alg (70:30) 2/24/18	20.7	5.935	14.765	12.5	13.7	1.76	1.69	5.68
LiPAA:Na-Alg (70:30) 2/24/18	21.6	5.935	15.665	13.3	13.7	1.86	1.80	6.03
LiPAA:Na-Alg (70:30) 2/24/18	22.9	5.935	16.965	14.4	13.7	2.02	1.95	6.53
LiPAA:Na-Alg (70:30) 2/24/18	24.1	5.935	18.165	15.4	13.7	2.16	2.08	6.99
LiPAA:Na-Alg (30:70) 2/24/18	21.8	5.935	15.865	13.5	13.7	1.89	1.82	6.11
LiPAA:Na-Alg (30:70) 2/24/18	17.8	5.935	11.865	10.1	13.7	1.41	1.36	4.57
LiPAA:Na-Alg (30:70) 2/24/18	21.2	5.935	15.265	13.0	13.7	1.82	1.75	5.88
LiPAA:Na-Alg (30:70) 2/24/18	19.3	5.935	13.365	11.4	13.7	1.59	1.53	5.15
LiPAA:Na-Alg (60:40) 2/24/18	22	5.935	16.065	13.6	13.7	1.91	1.84	6.18
LiPAA:Na-Alg (60:40) 2/24/18	24.5	5.935	18.565	15.8	13.7	2.21	2.13	7.14
LiPAA:Na-Alg (60:40) 2/24/18	22.4	5.935	16.465	14.0	13.7	1.96	1.89	6.34
LiPAA:Na-Alg (60:40) 2/24/18	23.1	5.935	17.165	14.6	13.7	2.04	1.97	6.61
LiPAA:Na-Alg (40:60) 2/24/18	21.7	5.935	15.765	13.4	13.7	1.87	1.81	6.06
LiPAA:Na-Alg (40:60) 2/24/18	20.1	5.935	14.165	12.0	13.7	1.68	1.62	5.45
LiPAA:Na-Alg (40:60) 2/24/18	19.7	5.935	13.765	11.7	13.7	1.64	1.58	5.29
LiPAA:Na-Alg (40:60) 2/24/18	18.1	5.935	12.165	10.3	13.7	1.45	1.39	4.68
LiPAA 3/1/18	23.6	5.935	17.665	15.0	13.7	2.10	2.02	6.79
LiPAA 3/1/18	23.5	5.935	17.565	14.9	13.7	2.09	2.01	6.76
LiPAA 3/1/18	23.8	5.935	17.865	15.2	13.7	2.12	2.05	6.87
LiPAA 3/1/18	21.4	5.935	15.465	13.1	13.7	1.84	1.77	5.95
LiPAA 3/1/18	24.6	5.935	18.665	15.8	13.7	2.22	2.14	7.18

Na-Alg 2/1/18	19	5.935	13.065	11.1	13.7	1.55	1.50	5.03
Na-Alg 2/1/18	18.4	5.935	12.465	10.6	13.7	1.48	1.43	4.80
Na-Alg 2/1/18	17.4	5.935	11.465	9.7	13.7	1.36	1.32	4.41
Na-Alg 2/1/18	17.4	5.935	11.465	9.7	13.7	1.36	1.32	4.41
PVdF 2/3/18	15.8	5.935	9.865	8.4	13.7	1.17	1.13	3.80
PVdF 2/3/18	15.3	5.935	9.365	8.0	13.7	1.11	1.07	3.61
PVdF 2/3/18	15.1	5.935	9.165	7.8	13.7	1.09	1.05	3.53
PVdF 2/3/18	15.7	5.935	9.765	8.3	13.7	1.16	1.12	3.76

Table 6: Anode Creation Data

Date	Anode Name	Weight Graphite (g)	Weight C.B. (g)	Weight PVDF (g)	Mass of Solvent (g)	Height of Dr. Blade (um)	Total Weight (g)	Active Material Percent
3/5/2018	Graphite 1	0.4454	0.015	0.8032	0.2391	100	0.5006	0.890
3/5/2018	Graphite 2	0.4457	0.0151	0.8034	0.2353	130,150,170,180,200	0.5010	0.890

Table 7: Anode Sample Weight. Highlighted Samples were Paired with Corresponding Highlighted Cathode Samples in Full Cells

Anode Sample	Total Mass (mg)	Mass of Cu Foil (mg)	Mass of Cathode (mg)	Mass of Active Material (mg)	Diameter of Sample (mm)	mAh	mAh test
Graphite 1	32.2	29.875	2.325	2.1	13.7	0.77	0.75
Graphite 1	31.5	29.875	1.625	1.4	13.7	0.54	0.52
Graphite 1	31.4	29.875	1.525	1.4	13.7	0.51	0.49
Graphite 1	32	29.875	2.125	1.9	13.7	0.71	0.69
Graphite 2	35.6	29.875	5.725	5.1	13.7	1.90	1.85

Graphite 2	34.6	29.875	4.725	4.2	13.7	1.57	1.53
Graphite 2	34.4	29.875	4.525	4.0	13.7	1.51	1.46
Graphite 2	35.1	29.875	5.225	4.6	13.7	1.74	1.69
Graphite 2	35.8	29.875	5.925	5.3	13.7	1.97	1.91
Graphite 2	37.7	29.875	7.825	7.0	13.7	2.60	2.53
Graphite 2	37.1	29.875	7.225	6.4	13.7	2.40	2.33
Graphite 2	36.6	29.875	6.725	6.0	13.7	2.24	2.17
Graphite 2	38.1	29.875	8.225	7.3	13.7	2.74	2.66
Graphite 2	37.2	29.875	7.325	6.5	13.7	2.44	2.37
Graphite 2	37	29.875	7.125	6.3	13.7	2.37	2.30
Graphite 2	36.3	29.875	6.425	5.7	13.7	2.14	2.07
Graphite 2	36.9	29.875	7.025	6.2	13.7	2.34	2.27
Graphite 2	36	29.875	6.125	5.4	13.7	2.04	1.98
Graphite 2	37.7	29.875	7.825	7.0	13.7	2.60	2.53
Graphite 2	38.4	29.875	8.525	7.6	13.7	2.84	2.75
Graphite 2	37.9	29.875	8.025	7.1	13.7	2.67	2.59
Graphite 2	38.5	29.875	8.625	7.7	13.7	2.87	2.79
Graphite 2	37.3	29.875	7.425	6.6	13.7	2.47	2.40
Graphite 2	39.1	29.875	9.225	8.2	13.7	3.07	2.98
Graphite 2	34.8	29.875	4.925	4.4	13.7	1.64	1.59
Graphite 2	37.4	29.875	7.525	6.7	13.7	2.50	2.43
Graphite 2	36.9	29.875	7.025	6.2	13.7	2.34	2.27
Graphite 2	35.8	29.875	5.925	5.3	13.7	1.97	1.91
Graphite 2	35.4	29.875	5.525	4.9	13.7	1.84	1.78
Graphite 2	36.4	29.875	6.525	5.8	13.7	2.17	2.11
Graphite 2	34.9	29.875	5.025	4.5	13.7	1.67	1.62
Graphite 2	35.2	29.875	5.325	4.7	13.7	1.77	1.72
Graphite 2	35.4	29.875	5.525	4.9	13.7	1.84	1.78
Graphite 2	34.9	29.875	5.025	4.5	13.7	1.67	1.62
Graphite 2	34.4	29.875	4.525	4.0	13.7	1.51	1.46
Graphite 2	33.5	29.875	3.625	3.2	13.7	1.21	1.17

References

[1] G. Blomgren, The Development and Future of Lithium Ion Batteries, (n.d.). http://jes.ecsdl.org.proxy.lib.ohio-state.edu/content/164/1/A5019.short (accessed March 25, 2018).

[2] N. Nitta, F. Wu, J.T. Lee, G. Yushin, Li-ion battery materials: present and future, Materials Today. 18 (2015) 252–264. doi:10.1016/j.mattod.2014.10.040.

[3] Q. Zhang, Z. Yu, P. Du, C. Su, Carbon Nanomaterials Used as Conductive Additives in Lithium Ion ...: Ingenta Connect, (n.d.). http://www.ingentaconnect.com.proxy.lib.ohio-state.edu/content/ben/nanotec/2010/00000004/00000002/art00004 (accessed March 29, 2018).

[4] Z. Wei Seh, Q. Zhang, W. Li, G. Zheng, H. Yao, Y. Cui, Stable cycling of lithium sulfide cathodes through strong affinity with a bifunctional binder, Chemical Science. 4 (2013) 3673–3677. doi:10.1039/C3SC51476E.

[5] V. Etacheri, R. Marom, R. Elazari, G. Salitra, D. Aurbach, Challenges in the development of advanced Li-ion batteries: a review, Energy & Environmental Science. 4 (2011) 3243–3262. doi:10.1039/C1EE01598B.

[6] M. Armand, J.-M. Tarascon, Building better batteries, Nature. (2008). doi:10.1038/451652a.

[7] Su Xin, Wu Qingliu, Li Juchuan, Xiao Xingcheng, Lott Amber, Lu Wenquan, Sheldon Brian W., Wu Ji, Silicon-Based Nanomaterials for Lithium-Ion Batteries: A Review, Advanced Energy Materials. 4 (2013) 1300882. doi:10.1002/aenm.201300882.

[8] D.B. Le, Electrodes including polyacrylate binders and methods of making and using the same, US20080187838A1, 2008. https://patents.google.com/patent/US20080187838/en (accessed March 29, 2018).

[9] Pieczonka Nicholas P. W., Borgel Valentina, Ziv Baruch, Leifer Nicole, Dargel Vadim, Aurbach Doron, Kim Jung-Hyun, Liu Zhongyi, Huang Xiaosong, Krachkovskiy Sergey A., Goward Gillian R., Halalay Ion, Powell Bob R., Manthiram Arumugam, Lithium Polyacrylate (LiPAA) as an Advanced Binder and a Passivating Agent for High-Voltage Li-Ion Batteries, Advanced Energy Materials. 5 (2015) 1501008. doi:10.1002/aenm.201501008.

[10] R. Santhanam, B. Rambabu, Research progress in high voltage spinel LiNi0.5Mn1.5O4 material, Journal of Power Sources. 195 (2010) 5442–5451. doi:10.1016/j.jpowsour.2010.03.067.

[11] M. Contestabile, S. Panero, B. Scrosati, A laboratory-scale lithium-ion battery recycling process, Journal of Power Sources. 92 (2001) 65–69. doi:10.1016/S0378-7753(00)00523-1.

[12] D.L. Wood, J. Li, C. Daniel, Prospects for reducing the processing cost of lithium ion batteries, Journal of Power Sources. 275 (2015) 234–242. doi:10.1016/j.jpowsour.2014.11.019.

[13] W. Li, B. Song, A. Manthiram, High-voltage positive electrode materials for lithium-ion batteries, Chemical Society Reviews. 46 (2017) 3006–3059. doi:10.1039/C6CS00875E.

[14] N. Cuesta, A. Ramos, I. Cameán, C. Antuña, A.B. García, Hydrocolloids as binders for graphite anodes of lithium-ion batteries, Electrochimica Acta. 155 (2015) 140–147. doi:10.1016/j.electacta.2014.12.122.

[15] J.-T. Lee, Y.-J. Chu, X.-W. Peng, F.-M. Wang, C.-R. Yang, C.-C. Li, A novel and efficient water-based composite binder for LiCoO2 cathodes in lithium-ion batteries, Journal of Power Sources. 173 (2007) 985–989. doi:10.1016/j.jpowsour.2007.07.073.

[16] Q. Wu, S. Ha, J. Prakash, D.W. Dees, W. Lu, Investigations on high energy lithium-ion batteries with aqueous binder, Electrochimica Acta. 114 (2013) 1–6. doi:10.1016/j.electacta.2013.09.068.

[17] B. Nykvist, M. Nilsson, Rapidly falling costs of battery packs for electric vehicles, Nature Climate Change. 5 (2015) 329–332. doi:10.1038/nclimate2564.

[18] B. Dunn, H. Kamath, J.-M. Tarascon, Electrical Energy Storage for the Grid: A Battery of Choices, Science. 334 (2011) 928–935. doi:10.1126/science.1212741.

[19] M. Secchiaroli, S. Calcaterra, H.Y. Tran, S.J. Rezvani, F. Nobili, R. Marassi, M. Wohlfahrt-Mehrens, S. Dsoke, Development of Non-Fluorinated Cathodes Based on Li3V1.95Ni0.05(PO4)3/C with Prolonged Cycle Life: A Comparison among Na-Alginate, Na-Carboxymethyl Cellulose and Poly(acrylic acid) Binders, J. Electrochem. Soc. 164 (2017) A672–A683. doi:10.1149/2.0781704jes.

[20] B. Gendensuren, E.-S. Oh, Dual-crosslinked network binder of alginate with polyacrylamide for silicon/graphite anodes of lithium ion battery, Journal of Power Sources. 384 (2018) 379–386. doi:10.1016/j.jpowsour.2018.03.009.

[21] A. Guerfi, M. Kaneko, M. Petitclerc, M. Mori, K. Zaghib, LiFePO4 water-soluble binder electrode for Li-ion batteries, Journal of Power Sources. 163 (2007) 1047–1052. doi:10.1016/j.jpowsour.2006.09.067.

[22] X. Wang, E. Yasukawa, S. Mori, Inhibition of anodic corrosion of aluminum cathode current collector on recharging in lithium imide electrolytes, Electrochimica Acta. 45 (2000) 2677–2684. doi:10.1016/S0013-4686(99)00429-6.

[23] E.P. Murray, T. Tsai, S.A. Barnett, Oxygen transfer processes in (La,Sr)MnO3/Y2O3-stabilized ZrO2 cathodes: an impedance spectroscopy study, Solid State Ionics. 110 (1998) 235–243. doi:10.1016/S0167-2738(98)00142-8.

[24] S. Harris, A. Timmons, D. Baker, C. Monroe, Direct in situ measurements of Li transport in Li-ion battery negative electrodes - ScienceDirect, (n.d.). https://www-sciencedirect-com.proxy.lib.ohio-state.edu/science/article/pii/S0009261409015462 (accessed March 29, 2018).

[25] H. Buqa, M. Holzapfel, F. Krumeich, C. Veit, P. Novák, Study of styrene butadiene rubber and sodium methyl cellulose as binder for negative electrodes in lithium-ion batteries, Journal of Power Sources. 161 (2006) 617–622. doi:10.1016/j.jpowsour.2006.03.073.

[26] B. Lestriez, S. Bahri, I. Sandu, L. Roué, D. Guyomard, On the binding mechanism of CMC in Si negative electrodes for Li-ion batteries, Electrochemistry Communications. 9 (2007) 2801–2806. doi:10.1016/j.elecom.2007.10.001.

[27] J. Chong, S. Xun, H. Zheng, X. Song, G. Liu, P. Ridgway, J.Q. Wang, V.S. Battaglia, A comparative study of polyacrylic acid and poly(vinylidene difluoride) binders for spherical natural graphite/LiFePO4 electrodes and cells, Journal of Power Sources. 196 (2011) 7707–7714. doi:10.1016/j.jpowsour.2011.04.043.

[28] C.M. Julien, A. Mauger, K. Zaghib, D. Liu, High Voltage Cathode Materials, in: Rechargeable Batteries, Springer, Cham, 2015: pp. 477–509. doi:10.1007/978-3-319-15458-9_17.